ASSESSMENT OF HYDRAULIC PERFORMANCE OF THE EASTERN NATIONAL WATER CARRIER, NAMIBIA: FLUMES THREE TO FOUR

A THESIS SUBMITTED IN FULFILMENT

OF THE REQUIREMENTS FOR THE DEGREE OF

MASTER OF SCIENCE IN CIVIL ENGINEERING

OF

THE UNIVERSITY OF NAMIBIA

BY

MUKENDOYI A. MUTELO

200013599

APRIL 2019

Main Supervisor:	Dr. Joachim. W. Lengricht (Department of Civil Engineering, UNAM)
Co-Supervisor:	Dr. Rolf Baur (Department of Civil Engineering, UNAM)

DECLARATION

I, **MUKENDOYI A. MUTELO**, hereby declare that this study is my own work and is a true reflection of my research, and that this work, or any part thereof has not been submitted for a degree at any other University.

Date: 2018/09/07

Signature: 

The findings, interpretations and conclusions expressed in this study do neither reflect the views of the University of Namibia, Department of Civil and Environmental Engineering nor of any individual member of the Faculty of Engineering and Information Technology.

Table of Contents

LIST OF TABLES

LIST OF FIGURES

LIST OF SYMBOLS

1 and *2* are the downstream and upstream locations respectively

$1/z$ is the side slope at the water surface

A is the flow area

a_1, a_2 are the velocity weighting coefficients

α - Velocity head weighting coefficient

C is the contraction or expansion coefficient

D is the hydraulic depth in m

Fr Froude number

h_{ce} is the contraction or expansion loss

h_e is the energy head loss

h_f is the friction loss

g is the gravitational acceleration in m^2/s

K is the conveyance for a given subdivision of the channel cross-section

L is the discharge weighted length

n is the Manning's coefficient

Q is the discharge in m^3/s

Q_L Total leakage loss in m^3/day

R is the hydraulic radius in m

Re Reynolds number

S is the friction slope in m/m

$\bar{S}_f$ is the representative friction slope between two cross-sections

T is the top width of flow in m

V is the channel average velocity in m/s

V_1, V_2 are the average velocities at the cross-sections

ν - Kinematic viscousity

X is the horizontal coordinate of flow depth

y is flow depth in m

Y is the vertical coordinate

Y_1, Y_2 are the water depth at the cross-sections

Z_1, Z_2 - Channel bed elevation

ABBREVIATIONS

DWA - Department of Water Affairs

EG- Energy gradeline (as in Figure 4-1 etc)

ENWC – Eastern National Water Carrier

HEC-RAS – Hydraulic Engineering Centre River Analysis System

NamWater – Namibia Water Corporation

RS- River station

WS- Water surface elevation (as in Figure 4-1 etc)

DEDICATION

I give special thanks as well as dedicate this thesis to Serge Chikuto McSergio V.S. Muyoba for his words of encouragement and support during this endeavour. The engraving of his name in this piece of work is immortalisation of the role he played.

ACKNOWLEDGEMENTS

Firstly, I would like to thank the Almighty God for all of life's mercies, strength to complete this work and blessings for me to realise my dreams and future ambitions, AMEN.

Further acknowledgements and many thanks go to my supervisors, Dr. Joachim Werner Lengricht and Dr. Rolf Baur the time and energy invested in guiding and directing me in this thesis.

I would also like to thank the Department of Civil and Environmental Engineering for the studentship. I thank Dr. Adedayo Ogunmokun and Professor Frank Kavishe of the Faculty of Engineering and Information Technology for their role in this research. I thank my fellow students Mr. Dirk Coetzee and Ms. Oriri Rukoro for all their encouraging words and contributions.

I thank NamWater Corporation for granting me permission to perform my research work on their infrastructure. I particularly acknowledge the role played by Mr. Andre Mostert, Mr. Walto and Ms. Belinda Veii. I also thank Mr. Ewald Karamba in a special for all his contribution during data collection excursions.

My gratitude also goes to Serge Chikuto McSergio, my cousins Malumo Malumo, Kahundu Mukena-Maiba and Kachie Mutelo, my brother Lifasi, my friends Israel Iilende, Velonica Kaleinasho, Hilima Nanquila, Hendrina Lukas, Siyamana Mulele and Packs Panduleni Haimene. I thank these people for various contributions on a social level.

Finally I thank the Ministry of Agriculture Water and Forestry for student grant which made it possible for me to complete this program.

ABSTRACT

In response to drought impacts, water augmentation by developing more boreholes in the Grootfontein-Otavi karst area and increase the use of the Eastern National Water Carrier (ENWC) was prioritised. Hence, plans to increase water transportation should be based a sound understanding of the hydraulic behaviour of the ENWC. Thus, this study sought to utilise the HEC-RAS model for the primary objective of assessing the hydraulic performance of the section between flumes 3 and 4 i.e. evaluating the hydraulic behaviour of the ENWC and determining its maximum water transportation capacity using HEC-RAS as well as perform a rough estimate of leakage and evaporation losses. The results show that the mean Manning's roughness coefficients $n = 0.099$, 0.124, 0.028 and 0.038 were respectively found in Canal 1 and 2, and Siphon 1 and 2. An assessment of observed and the predicted water depth exhibited a very good agreement, that yielded an $R^2 = 0.997$. The estimated maximum capacity of the canal system between flumes 3 and 4 was found to be discharge $Q = 0.3$ m^3/s while the flows accommodated in different sections of the canal ranged from $Q = 0.3$ to 1 m^3/s. A variation of the roughness coefficients did not seem to noticeably alter the estimated maximum capacity or influence the water levels of the normal flow regimes. With respect to leakage losses, the majority of canal sections i.e. Canal 1, Siphon 1 and Siphon 2, had leakage losses of the order of 20% or more of mean discharge in those respective sections. Therefore, it can be deducted that the hydraulic state of the aqueduct is undesirable when compared to the roughness condition $n = 0.015$ of concrete-lined aqueducts. Hence robust strategies for operation and maintenance of the aqueduct are required.

Key words: ENWC, Hydraulic performance assessment, water supply sustainability, Manning's roughness coefficient, leakage loss, estimated maximum capacity

1. INTRODUCTION

1.1 Background of the study

Recent drought conditions, unfavourable climatic conditions and environmental concerns have adversely impacted on the state of water resources and sustainability of water supply in Namibia, especially on the vulnerable water sources for Greater Windhoek area. This has created water challenges relating to water shortage and poor water supply security for Windhoek and its surrounding towns. Therefore, water supply augmentation has been acquiring more importance as a strategy for water supply authorities to meet demand on both the short-term and long-term basis.

In order to ensure sustainability of such water supply augmentation strategies, future water resources planning needs to be based on the sound understanding of the changing dynamics of local water resources systems and, the reliability and efficiency of water transportation structures. Thus, it is important to utilise hydraulic formulae, numerical models or other scientific tools useful in performing hydraulic evaluations that increase knowledge in terms of efficient proper operation adaptation, maintenance and efficient utilisation of water carriers.

One of the water supply augmentation schemes for Greater Windhoek is the Eastern National Water Carrier (ENWC). This is a predominantly gravity driven canal system that is about 260 km long and is used for the transportation of water from the karst aquifer system in the Grootfontein-Otavi area of Namibia to Windhoek via von Bach Dam [1]. The development of the ENWC formed part of the National Water Master Plan of 1974

[1]. The ENWC infrastructure was built and commissioned in the mid-1980s by the Department of Water Affairs (DWA) [1] while its operation has since been taken over by the national water utility, NamWater.

Generally the hydraulic performance of aqueducts is known to vary over a lifespan, in response to factors such as change in internal surface roughness, sedimentation and biofouling among others [2]. As such, it is necessary to conduct hydraulic performance assessments in order to understand their present and future hydraulic behaviour in terms of total energy losses during transportation and how this influences their water transportation capacity or efficiency after they have been in operation for long period of time [3]. It is also important to evaluate the canal and inline structures requirements and design-based deficiencies, and how these work together to influence the aqueduct's capacity to handle future increases in flow.

1.1. Problem statement

The effect of drought conditions on water supply security have seen recent water augmentation initiatives centre on developing more boreholes in the Grootfontein-Otavi karst area and increase the use of the ENWC. The need to increase water transportation renders it vital to have a sound understanding of the hydraulic performance status of the ENWC. Achieving this, requires the accurate location of leakages on the canal system, quantification of the head loss during transportation of water and overall conduct a robust hydraulic performance assessment with the aid of a model.

Numerical models such as the Hydraulic Engineering Centre River Analysis System (HEC-RAS), has been commonly used in the analysis and simulation of hydraulic

behaviour of complex aqueducts. It has capabilities of modelling flow conditions of canal systems with inline siphons and check structures. Hence, this study seeks to utilise the HEC-RAS model and field data to assess the present hydraulic behaviour of the ENWC, the prevailing roughness parameters and related total energy losses, as well as the transportation capacity of the water carrier to carry enlarged flow conditions through iterative determination of the overflow hydrographs along the water carrier system.

1.2. Aim and objectives

The primary aim of this research work is to assess the hydraulic performance of the Eastern National Water Carrier. The specific objectives are to:

1. Evaluate the hydraulic condition of the ENWC with HEC-RAS model using Manning's roughness coefficients $n = 0.015$ as the comparative indicator of good condition for concrete-lined aqueducts
2. Determine the transportation capacity of the aqueduct by estimating maximum discharge Q in m^3/s using modelling
3. Estimate leakage in $m^3/s/km$ and total actual evaporation losses in m^3/day

1.3. Significance of the study

This study is significant in that it will contribute to knowledge on hydraulic performance of inverted siphons and open canal reaches of the water carrier and serve as a source of scientific information for future related research. It will also provide useful information to the relevant authorities in respect of asset management. Moreover, this research will provide supplementary water flow records that can be used in future studies. The findings

in this research will give insights and surface understanding on the hydraulic performance of other similar water carriers such as the Calueke.

1.4. Limitations of the study

There are no continuous flow records at inlet and outlet structures of the siphons because they are ungauged, as a result the discharge, water surface profile elevation and related information are absent. To overcome the limitations, this study has utilised available flow records on gauged sections and collected supplementary data during field excursions. Two field excursions only were possible due to time and financial constraints. Also, a team of two people including the primary researcher using only one flow gauging instrument for data collection. Therefore, the time of flow measuring between any two cross-sections was kept between 15 and 30 minutes to ensure comparability of data.

1.5. Delimitations of the study

The scope of this study is limited to applying the HEC-RAS model for the assessment of the hydraulic behaviour and performance of the ENWC. The focus study area lies between flumes 3 and 4, as such the rest of the ENWC and other similar water carriers will not be included in this study.

2. LITERATURE REVIEW

2.1 Overview of the design and functioning of water transportation structures

Aqueducts are the most commonly used water transportation structures, these include canals, pipelines, inverted siphons and tunnels. Such aqueducts can be comprised of both canal and pipe sections [2] and are designed to the required water carrying capacity. Therefore, canal systems serve to convey water at a desired discharge over a distance from the source to an end-user point. It is often the case that the end-use point is located far from the source, requiring a lengthy canal system for water transportation.

Over the entire length of the water transportation structure, open and closed tops may exist. For open-top structures such as canal sections, the open channel flow condition prevail. This flow is exposed to the atmosphere and thus has free surface formed due to an interface with atmospheric air. On the other hand, closed top structures such as inverted siphon sections operate under full flow conditions and essentially function to convey water by gravity across various obstructions such as rivers, valleys, natural depressions, roads, canals and railways among others. Generally, man-made hydraulic structures are designed and constructed with unvarying cross-section and a constant channel bed slope. In these channels, the roughness parameters of the channel is often well defined and the hydraulic properties can be controlled with check and inline structures to meet targeted design requirements [4].

In order to design water carrying structures as required, there are several hydraulic formulas that can be applied. These formulae relate the desired water carrying capacity to channel geometry i.e. shape, slope and the roughness of the channel surface [2], [5], [6]. Manning's equation is the most commonly used equation while the Darcy-Weisbach and Hazen-Williams equations are commonly applied to pressurized flow designs [7]. However, all these equation are applicable to the design of both open channel and closed channel flow carrying structures. Another facet in the design of water transportation structures pertains to determining the characteristics of flow using the Froude and Reynolds numbers [8], [9].

The Manning's equation is commonly used to for the design and dimensioning canals by relating the desired capacity to the channel geometry. This is an empirical equation for approximating uniform flow conditions and it is applicable to open channels and closed channels [2], [3], [6], [7], [10], [11]. The Manning's equation takes the following form when expressed in terms of discharge.

$$Q = \frac{1}{n} A R^{2/3} S^{1/2} \qquad \text{(Eq. 1)}$$

Where Q is the discharge in m^3/s, A is the flow area, R is the hydraulic radius in m, S is the friction slope in m/m and n in the Manning's roughness coefficient. When using the Manning's equation to relate the average velocity in the channel to the friction slope the equation can be of the form: $V = \frac{1}{n} R^{2/3} S^{1/2}$ (Eq. 2)

Where V is the average velocity of flow in m/s and the other terms are as defined above.

Given the velocity and applying the principle of continuity of mass, discharge can be expressed in terms of velocity and cross-sectional area flow, the continuity equation is expressed as follows:

$$Q = AV \qquad \text{(Eq. 3)}$$

2.1.1 Characteristics and classification of open channel flow

The flow condition in an open channel can be classified as steady, unsteady, uniform or non-uniform based on many different criteria used for the classification of both open and closed channel flow [10], [12]. One of the important criteria for flow classification is based on how depth of flow varies in time and space at a given cross-section. Using time as the criterion, then flow can be classified as steady-state i.e. depth of flow does not change with time such that [10], [12], [13]:

$$\frac{\partial y}{\partial t} = 0 \qquad \text{(Eq. 4)}$$

And unsteady state where the depth at a given cross-section varies with time is mathematically represented by:

$$\frac{\partial y}{\partial t} \neq 0 \qquad \text{(Eq. 5)}$$

When the flow condition is classified in terms of space, then a flow is classified as uniform if the depth of flow does not vary with distance such that:

$$\frac{\partial y}{\partial x} = 0 \qquad \text{(Eq. 6)}$$

On the other hand, it is classified as non-uniform if the depth varies with distance at any cross-section, yielding the mathematical expression of the following form:

$$\frac{\partial y}{\partial x} \neq 0 \qquad \text{(Eq. 7)}$$

.Where, y is the depth of flow at the cross-section, t is time and x is the space or position of the cross-section. Non uniform flow can either be classified as being either gradually or rapidly varied. Gradually varied flow is such that the depth of changes slowly with distance, while rapidly varied flow occurs when the depth of flow changes rapidly over a relatively short distance such as is the case with a hydraulic jump - or *gradually varied* - the depth of flow changes rather slowly with distance such as is the case of a check structure on the canal [12].

Steady uniform flow where depth is constant with both time and distance is the primary flow condition in open channel in which the gravity forces are in equilibrium with the resistance forces. This is also the flow condition that is conceptualised and used in the design of water transportation structures. However, steady non-uniform flow where depth varies with distance but not with time and maybe gradually varied or rapidly varied is another commonly encountered flow [4].

Reynolds and Froude number

The abounding condition of open channel flow is governed by viscosity effects and gravity relative to the inertia forces of the flow while surface tension has negligible influence in most open channel flow problems. Therefore, based on the ratio of viscosity forces to inertial forces, the flow may be classified as laminar, transitional or turbulent [8], [9].

The flow is laminar if the viscous forces are so strong relative to the inertial forces that viscosity plays a significant part in determining flow behaviour. In laminar flow, the water particles appear to move in definite smooth paths, or streamlines, and infinitesimally thin layers of fluid seem to slide over adjacent layers. The flow is turbulent if the viscous forces are weak relative to the inertial forces [10], [12], [14]. In turbulent flow, the water particles move in irregular paths which are neither smooth nor fixed but which in the aggregate still represent the forward motion of the entire stream. A transitional flow is one which can be classified as neither laminar nor turbulent.

The measure of the ratio of .viscosity relative to inertia is represented by a dimensionless parameter known as Reynolds number which is defined as:

$$Re = \frac{4VR}{\nu} \qquad \text{(Eq. 8)}$$

Where Re is the Reynolds number, V is the average velocity of flow, R is the hydraulic radius in m and ν is the kinematic viscousity. Therefore, based on the Reynolds Number the flow condition is:

Laminar when $Re \leq 2320$

Turbulent when $Re \geq 2320$

The prevailing flow condition in most open channels is turbulent. This is due to the fairly small viscosity of water while having relatively large characteristic lengths. Hence laminar open channel flows are rare in real life. However, laminar open channel flow is known to exist, where thin sheets of water flow over the ground or where it is created deliberately

in model testing channels. Another characteristic of open channel flow is whether the condition is critical, subcritical or supercritical. Determining which of these states of flow is prevailing, is done by considering the role of gravity as a driving force in open channel drainage systems. The Froude Number is the actual parameter for determining how critical the flow condition is in a given channel. The Froude Number can be defined as a dimensionless parameter describing the ratio of inertial forces to gravitational forces [12] and it has the following mathematical form;

$$Fr = \frac{V}{\sqrt{gD}} \qquad \text{(Eq. 9)}$$

Where is the Froude number, V is the velocity of flow, D is the hydraulic depth and g is the acceleration due to gravity. Hence, based on the Froude Number the flow condition is:

Subcritical when $Fr \leq 1$

Critical when $Fr = 1$ and

Supercritical when $Fr > 1$

Subcritical occurs when the gravitational forces are the domineering drivers of the state of flow. The flow in this state is characterised by a relatively deep water level coupled with low velocities when compared to critical flow and the depth can be controlled by boundary conditions at a downstream location. In this case when a pebble is thrown in the water under subcritical flow backward formation of waves can be seen. Critical flow is unstable and theoretically the energy possessed by the flow is at a minimum for any given discharge. On the other hand, super critical flow is characterised by shallow water depth,

high velocity in comparison with critical flow conditions and the water depth is controlled at an upstream location. When wave generation is done in supercritical flow condition, then backward wave generation is limited or none. Given the nomenclature of the Reynolds and Froude numbers, the constituent parameters are described as follows

Hydraulic radius is expressed $$R = \frac{A}{P} \quad \text{(Eq. 10)}$$

Hydraulic depth is $$D = \frac{A}{T} \quad \text{(Eq. 11)}$$

Friction slope is $$S = \frac{h_f}{L} \quad \text{(Eq. 12)}$$

Where A is the area of flow, P is the wetted perimeter of flow, T is the top width of flow, h_f is the friction loss and L is the discharge weighted length.

2.1.2 Geometric properties of a parabolic section

The shape and general geometric properties of a parabolic canal cross-section are shown in Figure 2-1.

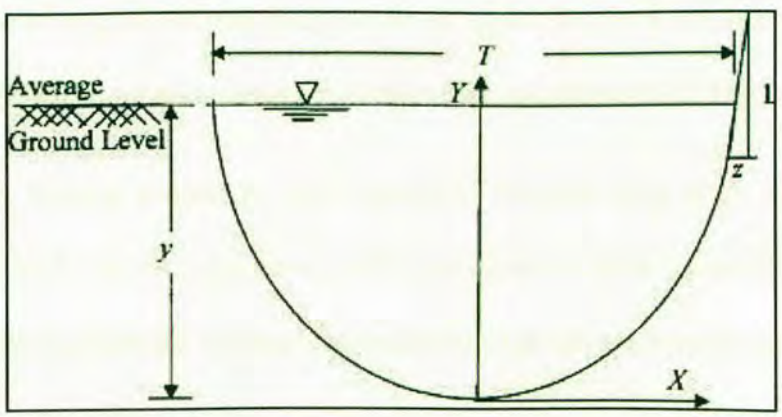

Figure 2-1 Morphology and geometric properties of a parabolic cross-section (Source: [15])

Taking into account the geometric properties of a parabolic-shaped canal shown in Figure 2-1, it can be shown that [15], [16]:

The flow area is given as $A = \frac{8}{3}y^2z$ (Eq. 13)

The wetter perimeter is $P = yF(z)$ (Eq. 14)

Where *F(z)* is given as $F(z) = 2z^2\left[\frac{1}{z}\sqrt{1+\frac{1}{z^2}} + ln\left(\frac{1}{z}+\sqrt{1+\frac{1}{z^2}}\right)\right]$ (Eq. 15)

Where z is the side slope at the water surface $Y=y$, Y is the vertical coordinate and y is the flow depth

2.2 Theoretical base of hydraulic models

Several models such as HEC-RAS, Storm Water Management Model (SWMM) and, MIKE 11 and 21 have been developed to aid the process of hydraulic analysis and perform flow simulation of open and closed channels. These models solve the mathematical problems that drive the physical properties of flow such as depth, velocity and discharge for the purpose of design, solving the problem of water flow and enhance understanding of the complex behaviour and response of hydraulic structures [17], [18].

Most hydraulic models, especially those applied to the modelling of the hydrodynamics of one dimensional flow such are based on the principles of Saint-Venant Equations [19]. These equations describe the gradually varied flow of an incompressible inviscid fluid.

Generally, the derivation of Saint-Venant Equations is based on the following overbearing assumptions [14], [20];

1. The flow is one-dimensional such that the main component of velocity u, is along the x-axis and is a function of x alone.

2. The fluid is Newtonian.

3. Forces causing the flow are due to gravity.

4. The water is considered as incompressible.

5. The flow condition is unsteady i.e. $\frac{\partial y}{\partial t} \neq 0$ (see Eq. 5)

The characteristics of flow through a conduit in space and time as represented in Saint-Venant Equations is conceptualised in Figure 2-2.

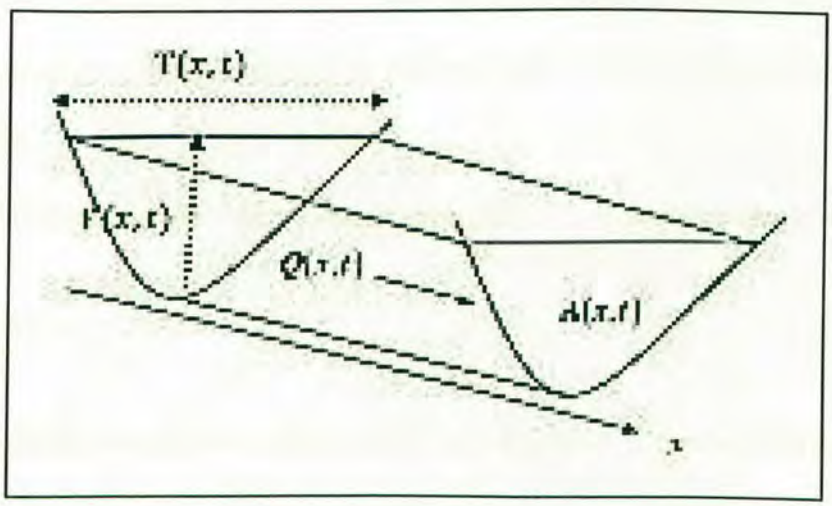

Figure 2-2 Characteristic variables of flow along a given channel length (Source:[21]*)*

Given a channel cross-section where x is the longitudinal abscissa and t is the time, then the characteristic variables of flow that should be considered in the model can expressed as follows [19], [20]:

A(x,t) is the wetted cross-sectional area in m^2

$Q(x,t)$ is the discharge at the cross-section in m^3/s

$V(x,t)$ is the average velocity in m/s

$Y(x,t)$ is the water depth in m,

$S_f(x,t)$ is the friction slope in m/m

$S_b(x)$ the channel bed slope and g the gravitational acceleration in m/s^2

Considering the described variable, the continuity equation in respect of discharge take the form:

$$Q(x,t) = A(x,t)V(x,t) \qquad \text{(Eq. 16)}$$

2.2.1 Governing equations

The Saint-Venant Equations are two-coupled hyperbolic partial differential equations [14], [22], [23]. The first of the couple being the conservation of equation and the second being the momentum equation which is derived from Newton's second law of motion along channel.

The continuity equation governing flow in open channels of arbitrary shape and size is:

$$\frac{\partial Q(x,t)}{\partial x} + \frac{\partial A(x,t)}{\partial t} = 0 \qquad \text{(Eq. 17)}$$

This is a differential equation that describes the transport of some kind of conserved quantity, in particular-mass. All examples of continuity equations express the same idea that the total amount (of the conserved quantity) inside any region can only change by the amount that passes in or out of the region through the boundary.

Since a conserved quantity cannot increase or decrease, it can only move from place to place. Then the general momentum equation for conservation of mass can be expressed as:

$$\frac{\partial Q(x,t)}{\partial x} + \frac{\partial}{\partial x}\left[\frac{Q^2(x,t)}{A(x,t)}\right] + gA(x,t)\left(\frac{\partial Y(x,t)}{\partial x} + S_f(x,t) - S_b(x)\right) = 0 \qquad \text{(Eq. 18)}$$

Momentum equations describe the motion of fluid substances and are derived from the Newton's second law of motion, together with the assumption that fluid stress is the sum of a diffusing viscous term (proportional to the gradient of velocity), plus a pressure term [20], [24]. These equations relate the sum of forces acting on an element of fluid to its acceleration. They generally exist non-linear partial differential equations and they operate together with supplemental equations (for example, conservation of mass) and well formulated boundary conditions, to model fluid motion accurately. The friction slope (S_f) parameter is modeled with the Manning's Equation such that if:

$$Q = \frac{1}{n}AR^{2/3}S^{1/2} \text{ (See Eq. 1), then } \quad S^{1/2} = \frac{Q\,x\,n}{AR^{2/3}} \qquad \text{(Eq. 19)}$$

$$\text{Therefore} \qquad S_f = \frac{Q^2 n^2}{A^2 R^{4/3}} \qquad \text{(Eq. 20)}$$

2.2.2 Initial and Boundary conditions

To complete the equations, we need to introduce initial and boundary conditions. The initial condition is given in terms of $(Q(x,0), Y(x,0))$, for all $x \in [0,L]$, with L as the length of the channel [9]. The choice of the boundary conditions depends on the flow characteristics, and the reverse also holds, since a change in the boundary conditions may change the flow characteristics. As mentioned above, it is possible to define different

boundary conditions according to the flow characteristics. The characteristic form of the equations is useful for understanding the different possible boundary conditions that one may define [14]:

- If the flow is subcritical, two boundary conditions are needed, one upstream and one downstream
- If the flow is supercritical, two boundary conditions must be defined at the upstream boundary
- For intermediate situations, i.e., when the flow in the channel is partly subcritical and partly supercritical, one may need to specify one, two, or three boundary conditions according to the situation

We can either choose the water depth or the discharge as a boundary condition.

There are therefore four possibilities:

1. Discharges at both boundaries: $(Q(0,t),Q(L,t))$. This corresponds to the case where two pumps impose the discharges at each boundary, where the canal is closed. This is the case that was mostly consider in this study, since it is assumed that the hydraulic structures such as the flume and inline structures can deliver a given discharge.

2. Water depths at both boundaries: $(Y(0,t),Y(L,t))$. This corresponds to the case of a body of water connected at each end to very large bodies of water. Such a situation can occur in deltaic zones, where a river can be connected to the sea at one end, and to a lake at the other end.

3. Discharge upstream and water depth downstream: $(Q(0,t), Y(L, t))$. This case corresponds to the case of a river where the upstream discharge is controlled by a dam, and the downstream ends up in a lake.

4. Water upstream and discharge downstream: $(Y(0,t), Q(L,t))$. This unusual case may correspond to a hydroelectric power plant controlling the downstream discharge of a river leaving from a lake.

2.2.3 Calibration of Saint-Venant Models

When faced with a practical problem of modelling an open channel, a hydraulic engineer usually requires the following data [14], [24]:

• Physical parameters describing the geometry of the open channel: slope, cross-section (shape, dimension, and variation along x).

• Value of the Manning friction coefficient. Usually, the geometry can be obtained with a measuring campaign, and the Manning coefficient can be either estimated from tables, or calibrated based on steady state water level and discharge measurements.

2.2.4 Method of solution

Typically, Saint-Venant Equations do not have a known solution in real geometry. As such the capabilities of numerical methods are often exploited for the provision of steady state solutions to Saint-Venant Models. The most commonly used numerical methods include the original method of characteristics, the Hartree and the Preissman implicit Scheme [22], [25], [26]. In other situations, Saint-Venant Equations can be modified into linear Saint-Venant Equations around a given steady state and subsequently, finite element methods and other numerical methods for solving linear partial differential equations can

be applied. Most 1D and 2D hydrodynamic models such as HEC-RAS are based on Saint-Venant equations.

2.3 Hydraulic modelling using HEC-RAS

When water carrying structures are in operation, there are several factors that influence their ability to maintain the design flow capacity or the same level of hydraulic performance of the over time. Generally, the hydraulic roughness encompasses the roughness of the channel surface and other variables [27], [28]. When water conveyance structures age, their surface lining steadily change, causing a slow increase in friction head losses over time due to increased pipe resistance [3], [6]. This equally applies to open channel situations especially to man-made aqueducts like in the case of the ENWC.

Other factors that diminish the hydraulic performance of many raw water conduits include the deposition of sediment loading, biofouling and inadequate cleaning. These factors tend to increase the friction losses especially when the raw water is abstracted from a surface water source [27], [29]. When the source of raw water is ground, the risk of sedimentation and biofouling is usually minimal.

However, when the source of raw water is rich in calcium, iron, magnesium and minute fluvial content as is the case with the Karst aquifers of Namibia, then the risk of calcium and magnesium precipitate and silt deposition increases especially in conduits that are highly prone to sediment deposition such as canals and inverted siphons. This is so, because the calcium and magnesium tend to react readily with oxygen to form precipitates [30], [31] that has to be cleaned out in the open canal section. This is equally true for raw water which is rich in iron, since dissolved iron is also readily oxidized by air, forming

precipitates with properties that alter the friction properties of surface of the aqueduct. However, in Namibia the water from the Karst aquifers is reportedly richer in calcium and magnesium content, thus the precipitates of these elements are envisaged to contribute to changes in the friction properties of

Therefore, when cleaning is not done, then the risk for such precipitates and sediment loading to settle on canal bed including the upward sloping pipe of inverted siphons become higher. Although cleaning can improve the roughness of the pipe for a period of time, the channel surface tend to get progressively degraded by the shear stress of water in motion [3], [7]. In this case, design of water conduits accounts for the natural degradation of the channel by estimating a friction factor for aging structures over time and how this affects future opportunities for further water resources development and the capacity for existing canals systems to carry significantly increased levels of discharge. Thus hydraulic model HEC-RAS can be applied to determine the hydraulic behaviour of canal systems.

2.3.1 Suitability of HEC-RAS for modelling canals

The available different hydrodynamic models have several overlapping functionalities but are also fundamentally different based on their inherent strength and limitations [32]. SWMM is a hydrological and hydraulic model that can perform 1D flow simulations, however, its inherent strength is on evaluation of urban storm water hydrology and hydraulic analysis of pipes and urban storm water drains. Therefore, while it can be useful for evaluation of canals and other conduits, it is more adapted for the simulation of quality and quantity of urban runoff [19], [32].

MIKE 11 is a 1D and MIKE 21 is a 2D model. Both these models are adapted for combined hydrological and hydraulic modelling needs [33]. This is because they have higher versatility and productivity and can handle complex systems. They are also fundamentally different from HEC-RAS based on the method of solution of the energy and momentum equations where MIKE uses an implicit finite different scheme to solve the energy and momentum equations [33], [34].

HEC-RAS is a Computational Fluid Dynamics (CFD) package developed by the U.S. Army Corp of Engineers (USACE). It offers suitable capabilities for both one-dimensional and two-dimensional hydrodynamic simulation. Steady flow water surface computations, movable boundary sediment transportation and water quality analysis can be simulated successfully using the one-dimensional functionality of HEC-RAS [21]. Unsteady flow simulation can be done both in one and two-dimensional components.

All simulations use a common geometric data representation as well as a common routine for both geometric and hydraulic computations. The inherent computational routines are well equipped to efficiently handle mixed flow (sub- and supercritical) regimes [35], [36]. Also, flow simulation using HEC-RAS allows for the integration of artificial channels, irregular-shaped and composite channels as well as steady or unsteady flow, and subcritical or supercritical flow regimes. With the aid of computational routines and dialog boxes, integration of bridges, culverts, check and inline structures, pump stations, basins, levees, flood plain encroachments into flow analysis can also be done [21], [36].

The Limitations of HEC-RAS are related to its inherent deficiencies in adequately handling multi-dimensional flow characteristics. HEC-RAS also tend to be ineffective

when applied to channels with steep bed slope i.e. slope that is greater than 10% [37], [38]. Also, when used on conduits with lidded cross-sections, the energy grade line can potentially lie outside the conduit which can result in stability challenges. However, HEC-RAS allows for setting larger-sized lids than the actual size of the conduit in order to accommodate the energy grade line within the channel [21].

2.3.2 Theoretical base of steady gradually varied flow

HEC-RAS is well adapted for performing one-dimensional water surface profile calculation for steady gradually varied flow in natural and constructed channels. This model can calculate water surface profiles representing a single flow regime i.e. subcritical or supercritical as well as for mixed flow regimes in a given channel shape [37]. The model uses a basic computational procedure for calculating water surface profiles that is based on solving the one-dimensional energy equation. In this case, the energy loses in the system are evaluated using resistance to flow representation of Manning's Equation and the contraction/expansion coefficients. The HEC-RAS model also integrates the momentum equation and utilises it as the overbearing computational procedure at the cross-sections where water surface profiles change rapidly [21], [23], [39].

Basic water surface profile calculations using the energy equations

The steady gradually varied flow water profiles in natural and artificial channels is well described by the steady, one-dimensional energy equations as graphically represented in Figure 2-3.

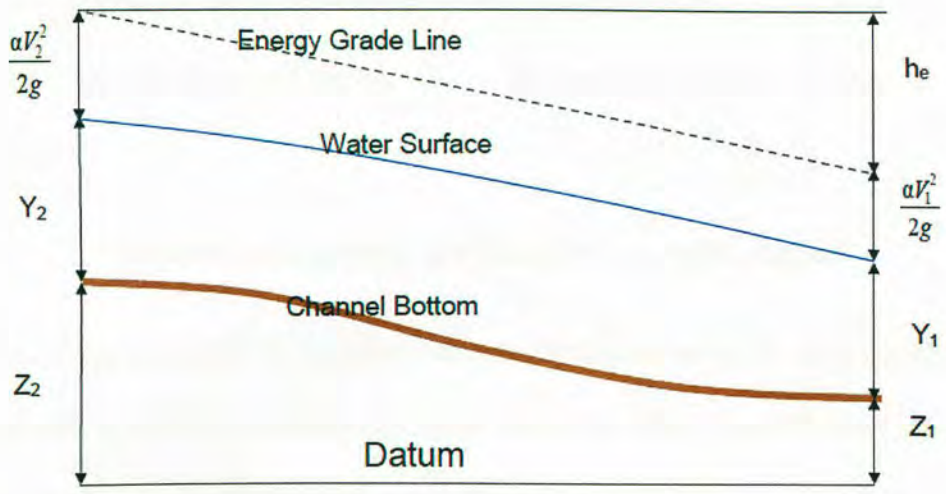

Figure 2-3 Schematic of the components of the energy equation (Source: [21]*)*

Aggregating the composite terms gives the energy equation which is expressed as follows:

$$Z_2 + Y_2 + \frac{a_2 V_2^2}{2g} = Z_1 + Y_1 + \frac{a_1 V_1^2}{2g} + h_e \qquad \text{(Eq. 21)}$$

The velocity weighting coefficients a_1, a_2 are used to modify the velocity head term when the velocity values varies significantly over a given cross-section. Hence, he stated energy equation is applied to open channel hydraulics in a modified manner. This results in the expression of the energy in respect of the basic approximations and relationships of its constituent components as seen in Figure 2-3. The components include the energy head loss, the velocity head and water surface profile. The energy head loss (h_e) between two cross-sections has the friction loss (h_f) and the contraction or expansion loss (h_{ce}) components and the equation is of the form:

$$h_e = h_f + h_{ce} = L\bar{S_f} + C\left|\frac{a_2 V_2^2}{2g} - \frac{a_1 V_1^2}{2g}\right| \qquad \text{(Eq. 22)}$$

The expanded form of the approximation and relationships of the associated terms in the energy head loss equation and the explanation is presented in the HEC-RAS Reference Manual [21].

Conveyance calculation and Manning's n in the channel

In the case of an artificial channel that have no over bank flow, the total conveyance is approximated as a single conveyance element in the main open channel. If there is overbank flow then the incremental conveyance elements in the overbanks are added to the total conveyance component. This approach to conveyance approximation is related to the discharge dominant Manning's equation of the form [21], [36]:

$$Q = KS_f^{1/2} \qquad \text{(Eq. 23)}$$

Where K is the conveyance for a given subdivision of the channel cross-section and it is evaluated based on the relationship:

$$K = \frac{1}{n} AR^{2/3} \qquad \text{(Eq. 24)}$$

The Manning's n-value which represent the resistance to flow is related to the channel surface roughness and Reynolds number and is approximated to a single value along the channel area. In the case where varying roughness regimes exist in the channel, HEC-RAS adapts its calculation approach and integrates composite Manning's n-values that represent the roughness in different channel subdivisions at a given cross-section.

Evaluating the Mean kinetic Energy Heard

Another dominant component of the energy equation is the velocity head. Approximating the mean kinetic energy head requires can be approximated as a discharge weighted velocity head after a velocity head weighting coefficient has been determined [21]. The equation for mean kinetic energy head approximated from discharge weighted velocity head is represented by the relationship:

$$\alpha\frac{\overline{V}^2}{2g}=\frac{Q_1\frac{V_1^2}{2g}+Q_2\frac{V_2^2}{2g}}{Q_1+Q_2}=\frac{\frac{1}{2g}\left(Q_1\frac{V_1^2}{2g}+Q_2\frac{V_2^2}{2g}\right)}{Q_1+Q_2} \qquad \text{(Eq. 25)}$$

Where α is the velocity head weighting coefficient

$\alpha\frac{\overline{V}^2}{2g}$ is the term representing the Mean Kinetic Energy in the system

The right side of the equation represents the discharge weighted velocity head. The whole equation can be re-written, yielding the practical equation for evaluating the velocity head weighting coefficient, therefore:

$$\alpha=\frac{Q_1V_1^2+Q_2V_2^2}{(Q_1+Q_2)\overline{V}^2} \qquad \text{(Eq. 26)}$$

The associated iteratively determined steps for driving the above said relationship as well as alternative methods for computing the velocity head weighting coefficient are presented in details in [21].

Evaluating friction losses in the system

In principle the friction losses are evaluated as the product of the representative friction slope between two section and the discharge weighted reach lengths. On the other hand, the slope of the energy grade line is determined from a relationship of the Manning's equation and is expressed as [21]:

$$S_f = \left[\frac{Q}{K}\right]^2 \qquad \text{(Eq. 27)}$$

Contraction and expansion losses

The approach for computing contraction or expansion losses is based on the assumptions that there is a contraction in channel cross-section whenever the system velocity head at a downstream is greater than the velocity head upstream. Also, whenever, the velocity head at an upstream location is greater than the velocity head downstream, an expansion of the channel is assumed. The procedural equation for evaluating contraction or expansion losses is as follows [21]:

$$h_{ce} = C\left|\frac{\alpha_1 V_1^2}{2g} - \frac{\alpha_2 V_2^2}{2g}\right| \qquad \text{(Eq. 28)}$$

Where C is the contraction or expansion coefficient. Typical *C*-values associated with various channel cross-section transitions and the effect of varying controlling structures are presented extensively in [20].

Critical depth evaluation

The critical water surface elevation exists at the elevation where the total energy head in the system is at a minimum. The process for evaluating the critical depth follows an iterative procedure that begins with assuming a range of water surface elevation values and subsequently evaluate the corresponding energy head [21], [40]. The water surface elevation that yields the minimum total energy head is the critical depth. This is evaluated based on the total energy head equation expressed as:

$$H = WS + \frac{aV^2}{2g} \qquad \text{(Eq. 29)}$$

Where WS- Water surface elevation. Furthermore, the assumptions that need to be satisfied for critical depth to be computed are stated in [21].

Weir equations

Flow across inline weirs is evaluated as either ungated or gated weirs. The standard equation of flow across all weirs is expressed as [21], [41]:

$$Q = CLH^{3/2} \qquad \text{(Eq. 30)}$$

Where C is the weir coefficient, L is the weir length and H the energy head loss. The weir coefficient is a lumped parameter that include the discharge coefficient C_d and it is approximated based of the following relationship:

$$C = \frac{2}{3} C_d \sqrt{2g} \qquad \text{(Eq. 31)}$$

The actual application of the standard weir equation is slightly different for ungated weirs compared to gated weirs. The computation approach for ungated inline broad crested weirs is such that the analyst has to specify a weir coefficient and HEC-RAS subsequently performs an automatic calculation of the submergence reduction of discharge. On the other hand, when modelling ungated weirs, the analyst can specify a weir coefficient for flow over the weir when the gate is completely open.

Computation procedure for solving the energy equation

The procedure for calculating water surface profile for subcritical flow is such that the iterations begin from the downstream end to the upstream. Water surface profiles for supercritical flow are computed starting from upstream to a downstream location. Depending on the flow condition, the steady state computation procedure begins by assuming an initial water surface profile at an upstream or downstream cross-section. This is followed by determining the K value and the velocity head corresponding to the initial water surface profile [21], [36]. The calculated K value and the velocity head are used to determine the representative friction slope between the cross-sections and also evaluate the energy head loss equation. The next step is to solve the energy equation for the generation of simulated water surface profiles. These water profiles are compared to the initial profile and the steps are iteratively repeated based on built-in criteria until when the values agree to a specified tolerance level.

Using the Momentum equation

Whenever there is a condition of rapid variation in flow and the characteristic water surface profile passes through the critical depth, the energy equation becomes no longer applicable. For these flow conditions, HEC-RAS solves the ensuing water flow problem for one-dimensional simulation by utilising the momentum equation [21], [36].

Boundary conditions

Boundary conditions are always introduced in the computation procedure in order to ensure efficiency and completeness of equations used in calculating water surface profiles. Boundary conditions are such that they define the starting water level at the furthest downstream end, which is the first step of the water surface profile calculation procedure in the HEC-RAS model [24], [21].

The choice of boundary conditions is influenced by flow characteristics in the channel, however, the most commonly applied boundary condition is the normal depth[21]. This condition is obtained automatically in the model by applying the energy slope and Manning's equation to approximate the normal depth. The normal depth boundary condition has been reported to introduce errors to the vicinity of the boundary station. Therefore, to overcome these deficiency, it is suggested that the boundary station be placed far enough i.e. over 1500m from the study area to remove the boundary condition based uncertainties. If the system that is being analysed is not long enough to make such allowance, then a visual or sensitivity analysis to establish the degree of introduced errors.

Other possible boundary conditions include the critical depth, rating curve, stage and flow hydrographs or a combination of the stage and flow hydrographs [42], [43].

Validation of the Model

This process is undertaken in order to check the accuracy of the model's presentation of the flow problem being analysed and ascertain that the results produced are within a satisfactory range of accuracy. The validation procedure uses observed data and other means possible to test the validity of HEC-RAS application to flow characteristics in a given channel [21]. This process involves controlling as many parameters as possible to determine which parameters effect model accuracy. Some of the model parameters that are often controlled include Manning's roughness coefficient and channel geometry [44].

2.3.3 Overview on application of HEC-RAS for hydraulic modelling of aqueducts

The coupled 1D and 2D HEC-RAS model has been widely applied for the simulation of flow conditions and hydraulic parameters in large river systems [35]–[39] and complex multi structure aqueducts [46], [47]. HEC-RAS has found wide application the field of flood modelling. It has also been used for characterization of roughness parameters of rivers by calibrating the model against observed flow discharge and water level [48].

The HEC-RAS model have been globally applied in benchmark test against several other numerical models and have been found to perform well [37], [49]. It has also be used in sensitivity analysis of roughness and other model inputs for both rivers and canals. In evaluating aqueducts, HEC-RAS has been found to simulate observed transient flow

conditions, predicting velocities and water surface profiles and the general hydraulic behaviour of complex multi-hydraulic structures [37], [49], [50].

HEC-RAS has been used in the evaluation of canal hydraulics under steady state and rapidly varied flow, where it been used as a basis for improved canal performance management [46]. This has been achieved due to HEC-RAS capabilities of simulating effective roughness parameters on both the canal, inline structures and siphon reaches [47]. Further advancement in its application has seen acceptable use in the evaluation of sediment transport, water quality, blockage of bridges [42], [51] and estimation of discharge coefficients of inline weirs and other structures [47].

3. METHODS

3.1 Description of the study area

The Eastern National Water Carrier, Grootfontein to Omatako section is an approximately 260 km long gravity driven canal system that lies completely within the Otjozondjupa region of Namibia [1] as shown in Figure 3-1. The canal system is comprised of open canal reaches that are connected by a series of inverted siphons (see Figure 3-2) of different lengths. Along the entire canal reach there are six partial flumes which serve as stations for flow gauging and monitoring.

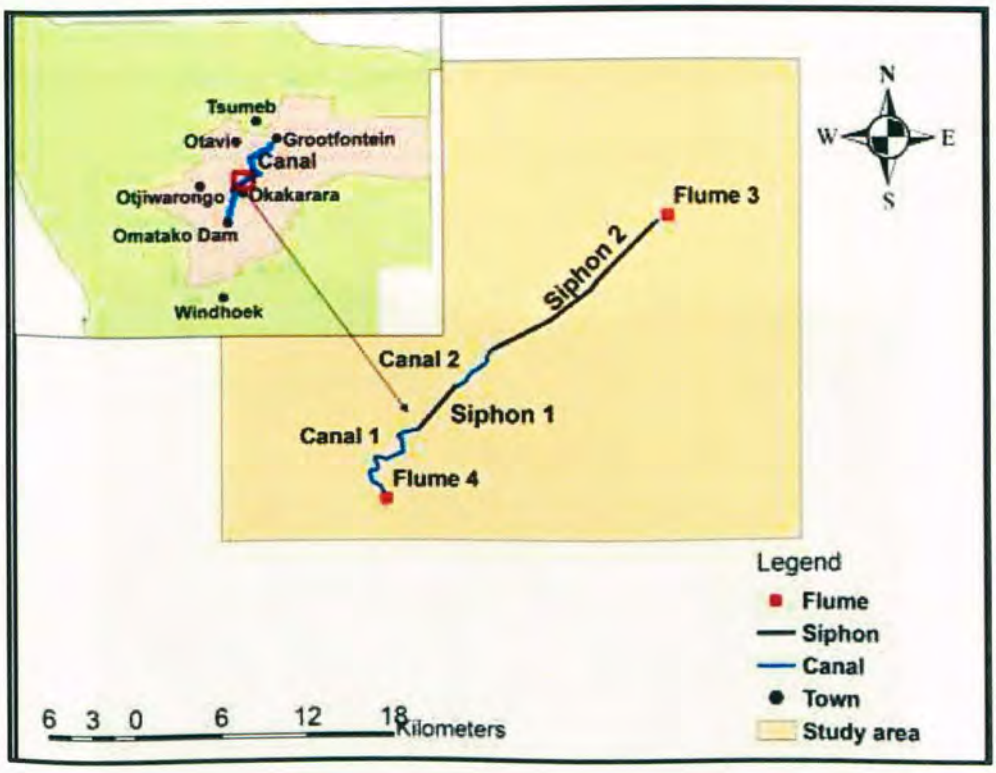

Figure 3-1 Location of flumes 3 and 4 on ENWC

In this study, the canal section between flume 3 and flume 4 represented the area of interest. The section of the canal stretch between flumes 3 and 4 was about 30 km

long. Flume 4 lies approximately 50 m from the off take to Okakarara Water Treatment plant and about 10 kilometres from the Okakarara Town while flume 3 lies about 30 km upstream.

After a running for approximately 30 m from partial flume 3, the canal culminates into an inverted siphons as shown in Figure 3-2, and this siphon runs underground for approximately 14 km. After crossing the D2512 gravel road from Waterberg to Grootfontein, the open canal re-emerges again and extend for a distance of over 4km from the siphon outlet before it converges into a another siphon reach which links the last open canal that runs for over 7 km to the Okakarara off take and partial flume 4 and the after the canal system proceeds to Omatako Dam via flume 5 and 6.

Figure 3-2 Open canal section at flume 3

Some key features of the open canal section include a presence of broad crested long crested weirs of a duckbill type. These long crested weirs are used to regulate flow along the canal especially at sections that where the canal culminates into an inverted siphon reach. In general, the long crested weirs are placed at a distance of 2.2 to 2.9 km from the upstream long crested weir. Flow conditions immediately downstream of long crested weirs is characterised by shallow fast flowing water that gradually changes to deep slow flow as the distance from the upstream weir increases. As such, it can be said that mixed flow conditions exist in the canal.

During the course of the year, the canal is operated under two different flow regimes i.e. low flow and higher flow regimes. During the low water flow regimes the canal carries low levels of discharge that is transmitted to only meet for the water consumption demand of Okakarara town. Under these flow conditions, large sections of the canal bed downstream of partial flume 4, often remain dry or have very shallow pools of water.

Water demand in Okakarara town is driven by household water consumption needs of a population of 7000 with an annual growth rate of 4% based on the National Population Census of 2011 [52]. In 2013, the Town Council envisaged a water demand increase by nearly threefold with 2 to 5 years due to the intermediate to long-term strategic development plan. Water demand was envisaged to be increased by the proposed development of lighter, heavy and agronomic industries and the expansion of low-income, middle and upmarket housing [53].

During the dry season, the canal is operated under increased flow regimes to augment water supply to the Greater Windhoek area as part of the three dam system. The length of this period varies based on the nature of the rainfall year and how acute the water shortage situation is. However, in the past the period often run between September and February. Under these flow regimes, the canal transmits flow from Grootfontein to Omatako Dam. The elevated discharge in the canal during this period is often driven by the need to meet the water supply demand for Windhoek and its satellite towns. Windhoek is the administrative capital, economic and employment hub and has a population growth of 4.4% per year [52].

Topography, vegetation and hydrology

The regional terrain in Otjozondjupa is relatively flat with few solitary mountainous features, sand dunes and valleys [54]. The most prominent objects of the landscape are the Waterberg Plateau and the Omatako Mountains. The general elevation undulates gently in the range between 4956 and 4619 feet above sea level. The most dominant soil type is the Kalahari sand with parts of sandy loam and loamy soils. The vegetation is characterised by broad-leaved deciduous trees and thorny species [54]. Thorn bush savanna is the most opportunistic and invasive tree species in those areas prone to encroachment of bushes.

Annual rainfall in Otjozondjupa region ranges between 300 and 400 mm and this is received during a rain season that extends from November to April. The rainfall profile varies from south to north and in the Northern part there is higher rainfall zone caused by an orographic uplift over the hills in the Goortfontein-Komabt-Tsumeb area [55].

This area is underlain by karst aquifers which are the primary source of water fed into the ENWC. The region has small to large ephemeral rivers, where some of the rivers feed their discharge into the Omatako Dam. The potential evaporation over the region varies between 2800 and 3200 mm per year [55], resulting in a rainfall deficit of 2400 to 2900 mm annually.

3.2 Research design and sampling

In order to satisfy the objectives of this study, a modelling research design was adopted. This said research design was implemented by utilising the hydraulic model HEC-RAS for the simulation and evaluation of the hydraulic behaviour of ENWC canal in this study.

In this research a convinient sampling approach was used and this was found to be the most suitable approach for ensuring a balance between the characteristics of the population and the objectives of the sudy. Therefore, along Open Canal 1, the sampling points where flow gauging was done were those points immediately upstream and downstream of the long crested weir. Thereafter, flow recording was done at cross-sections that located at 300 m intervals. Sampling in the Open Canal 2, was also done at the upstream and downstream of the long crested weirs and after that at cross-sections located at distance of 450 to 500 m from the preceding cross-section. Other points of interest where flow was recorded were at the inlet and outlet structures of the inverted siphons.

In terms of defining the channel cross-section intervals for inputing in the canal system in HEC-RAS model, cross-section were defined to lie at distance interval of 150 m from the previous cross-section while a distance interval of 300 m was preferred for cross-section

description in the inverted siphon reaches. This resulted in 137 interpolated cross-sections and 10 user defined cross-sections.

3.3 Justification of using HEC-RAS

While HEC-RAS tends to be inefficient when applied to steep bed channels, this conditions did not apply because the canal system studied had a slope of less than 0.6% which is highly gentle. In addition, HEC-RAS is found in the public domain yet the process to model canal systems with a series of inverted siphons incorporated as lidded cross-sections is less tedious resulting a generally simpler workflow compared to alternate public domain and proprietary models.

Furthermore, the unavailability of data records on certain parameters, rendered modeling using computational abilities of HEC-RAS as the most efficient and comprehensive approach compared to spreadsheet calculations. Moreover, in the case of mixed flow or where water surface profiles vary rapidly, HEC-RAS is responds by switching the over-bearing principle to the momentum equation. This creates opportunities to respond appropriately to the influence of hydraulic structures such as long crested weirs during the process of flow simulation.

3.4 Research instruments

For successful completion of the project, the following instruments were used:

- 20 m measuring tape, located at NamWater was used to measure geometric characteristics of broad crested weirs, and to determine distance at which flow velocities were recorded at a given cross-section

- GPS was used to capture geographic positions of the cross-section and structures where flow gauging was done
- Car was required for transportation along the canal during the field excursion
- A gauge plate was used for measuring the sediment sludge or pipe pressure variation
- NTECH current meter located at NamWater was used for measuring discharge and flow velocity
- Notebook was used for noting field observation, data and comments
- A ladder was used for getting in and out of the canal
- A camera was used to take pictures of notable features of the canal

3.5 Measuring discharge and water level

Discharge and water levels were recorded during a field excursion starting at partial flume 4 going upstream to flume 3. In order to obtain water level information at the desired cross-section, a portable 1m long gauge plate was used to take readings of the water stage at the midpoint of the canal. In the case where the water stage hydrograph was higher than 1 m, a second 0.5 m water level gauge plate was used together with the first level meter. On the other hand, discharge was taken indirectly as a measure of velocity and wetted area of flow in a parabolic cross-section. This was done by recording flow velocities with the aid of a NTECH flow meter. At each cross-section, flow velocities were recorded at the distances 0.9, 1.7 and 2.5 m from the right-sided wall of the canal. These distance intervals were seen as representative of the areas of varying velocities profiles at such cross-sections. Subsequently, the discharge (Q) was calculated the using continuity equation:

$Q = AV$ (See Eq. 1)

The wetted area of in a parabolic cross-section was obtained using the equation:

$$A = \frac{2}{3} yT \qquad \text{(Eq. 32)}$$

Where A is the area of flow, y is the depth of flow and T is the top width of flow.

3.6 Channel geometry

The channel bed elevation and slope information were extracted from the invert level charts that are located at NamWater HQ, Civil Engineering Division.

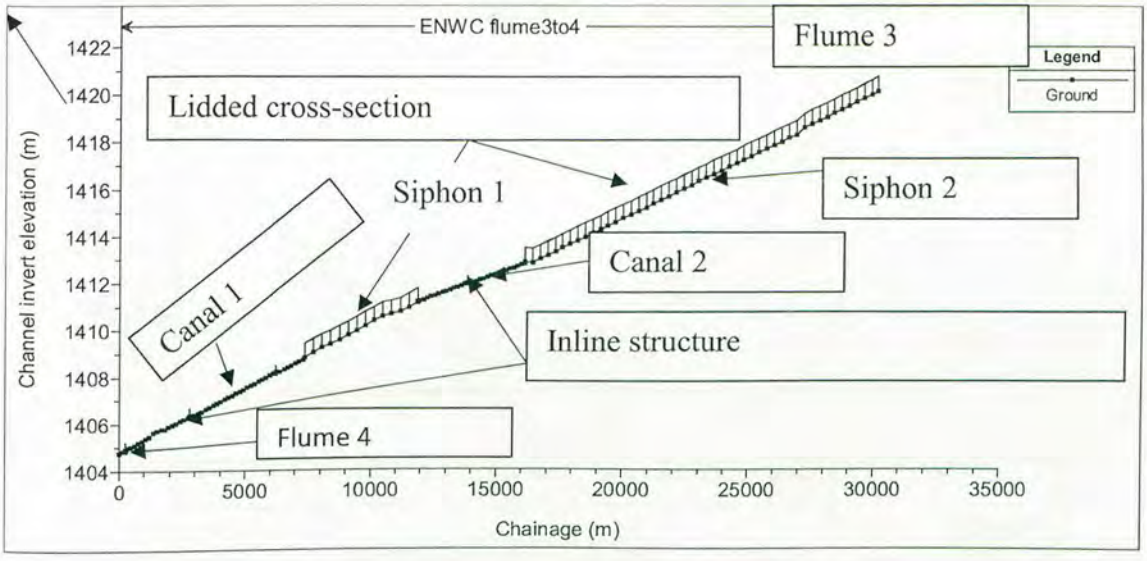

Figure 3-3 Channel bed elevation profile and slope

Figure 3-3 shows HEC-RAS model representation of the channel bed elevation, slope profile and chainage of the canal system between flumes 3 and 4. There is a 17m drop in elevation, which is equivalent to a channel bed slope of 0.580 m/km. The channel elevation profile also shows the location of inline structures and, that of the open Canal 1 and 2 which are separated by Siphon1. It also shows the profile of lidded cross-sections

which depict the presence and location of siphon 1 and 2 on the canal flumes between flumes 3 and 4.

The shape profile of the open canal and lidded cross-sections as graphically represented in the HEC-RAS model is shown in Figure 3-4 (a) and (b). HEC-RAS model typically accounts for each channel cross-section as a river station (RS) while a river station number represents the location of the cross-section on the channel reach. Therefore, in Figure 3-4 (a) and (b) the values 0.015 ad 0.005 are the Manning's roughness coefficients at the given cross-sections.

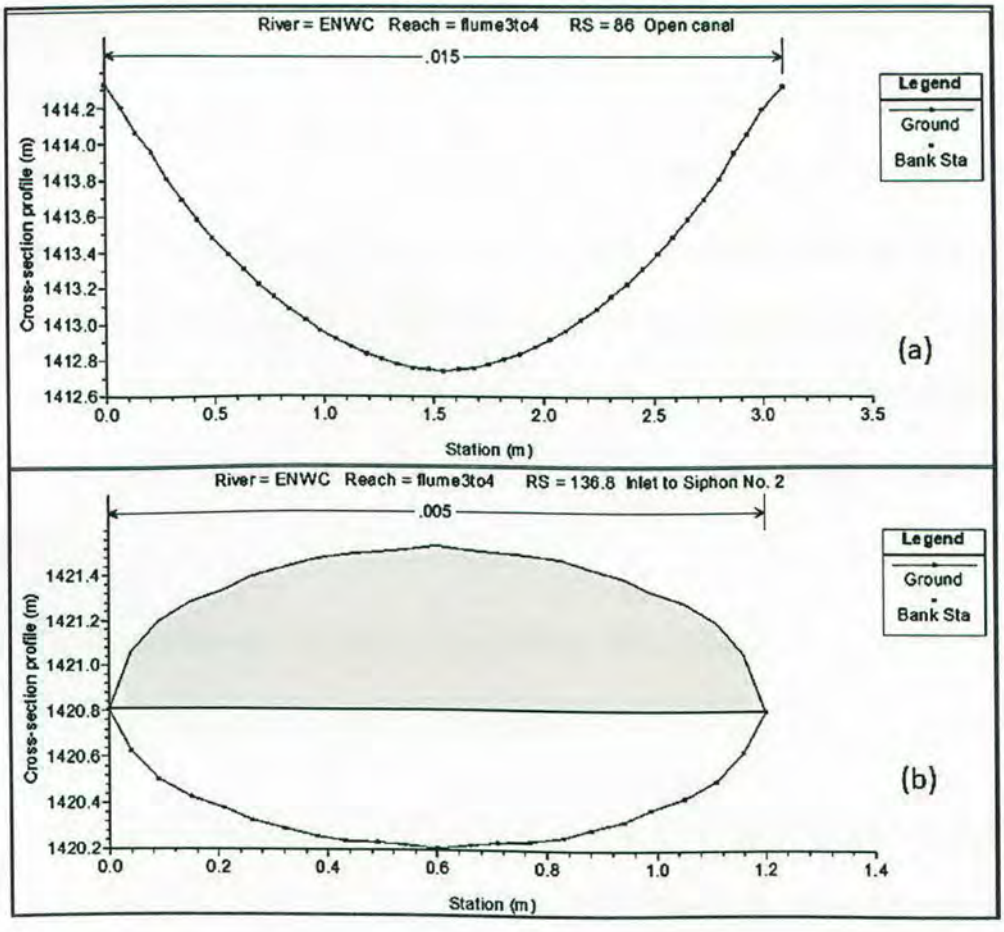

Figure 3-4 Cross-section profile of the canal (a) open parabolic canal (b) inverted siphon as a lidded cross-section

Channel cross-section geometry information in respect of the size, shape and channel bed elevation profile at each cross-section station were obtained through field measurement. The channel bed elevation profile of the open canal cross-section was measured at 0.07 m interval from left to the right-sided station. The elevation profile of inverted siphon cross-sections was measured at 0.04 m intervals as seen in Figure 3-4(b). It can also be seen from the cross-section geometry that the topwidth of the open canal was 3.1 m and having a depth of approximately 1.57 m along the stretch between flumes 3 and 4.

The aqueduct has a series of inverted siphons of the circular type that have a diameter of 1.2 m. Therefore, the top half of the inverted siphon, which began at the depth of 0.6m to 1.32 m was taken as the lid on the cross-sections comprising the siphon. In order to ensure that the energy grade line did not lie out of the channel based on model requirements, the maximum level of the lidded cross-section was increased based on trial and error, and it was found that an increase of 10% was sufficient and this yielded a maximum depth of 1.32m for the lidded cross-section. Other recorded geometry information included long crested weirs parameters such sluice gate size, flow depth of weir and side wall dimensions.

3.7 Setting-up and calibration of HEC-RAS model

3.7.1 Setting-up the HEC-RAS model

After gathering all the data required for the successful performance of hydraulic modelling, the HEC-RAS model was set-up by using the base geometric data functionalities. This process started with drawing the canal system geometry schematic from a Google Image (Appendix A). Subsequently 10 user defined and 137 interpolated

cross-sections were entered on the channel schematic. The cross-section interval of 150 and 300m were maintained for the open canal and inverted siphon reaches respectively. The cross-section schematic is shown in Appendix B.

The cross-section data and Manning's n-values were entered using the edit and create cross-section function in the geometry data editor. A hand calculated Manning's n-value of 0.057 $s^{1}.m^{-1/3}$ was used as the initial roughness coefficient and subsequently the model was calibrated against the observed stage hydrograph. Inverted siphons were added and modeled as a series of cross-sections with lids while broad crested long weirs were added using inline structures. The complete procedure for performing this task is contained in [21].

The next step was to specify the channel flow conditions. In this case, the flow data editor was used to enter flow hydrograph at the upstream end as well as observed data at the appropriate cross-sections. Since a mixed flow condition was modeled, boundary conditions were specified at both the downstream and upstream end. The normal slope of 0.58m/km slope was used for the downstream boundary condition while a known water surface elevation was used as upstream boundary condition.

3.7.2 HEC-RAS model calibration and validation

The effective Manning's roughness coefficients were estimated through the procedure of model calibration. This was done on a trial and error basis where the initial n-value of 0.057 was used and subsequently varied iteratively until when n-values that produced a

great degree of agreement between the first set of observed data and predicated water surface profiles.

The Manning's n-values found through the calibration procedure were taken as the effective roughness parameters describing the hydraulic behaviour and response of the canal. Subsequently, the model was validated a second set of observed data collected during the low regime flow in the ENWC: flumes 3 to 4.

3.8 Determining the rate of evaporation

To determine the daily average daily potential evaporation rate. Spatially based national average evaporation isolines were visualised in Arc Map 10.1. This spatially based data is empirically derived and assembled as an annual average of highly variable inter-monthly evaporation rates. Since, in the development of this national data set, a correction for monthly variations was performed, it was assumed that this measure of evaporation rate was relevant. Furthermore, the isolation of conditions influencing rate of evaporation rate was not done.

Therefore, in this study, focus was placed on performing a spatial interpolation as shown in Figure 3-5, and there after perform a simple conversion from annual potential to mean daily potential evaporation rate which was taken as representative of the average maximum daily evaporation rate over the open canal. Subsequently, the computed spatially distributed annual evaporation rate for Otjozondjupa region was extracted and converted to average daily evaporation rate from the national potential evaporation map by applying basic mathematical function and unit conversions.

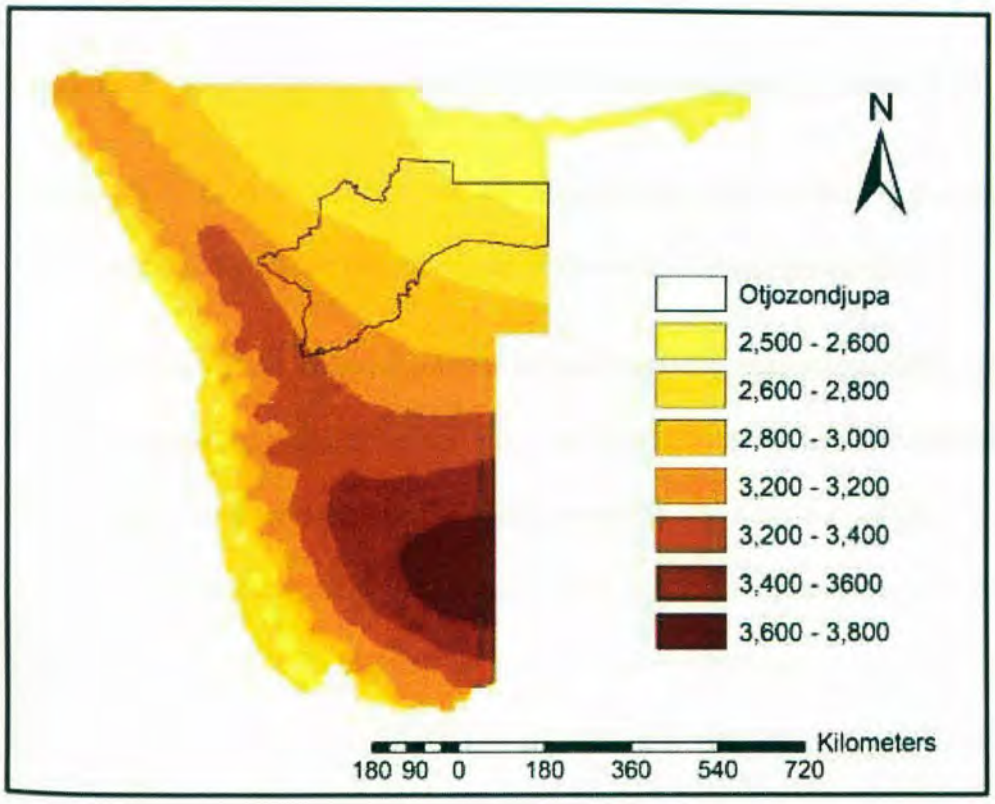

Figure 3-5 Evaporation map of Namibia with Otjozondjupa region insert

Figure 3-5 shows that the Otjozondjupa region lies predominantly in zone where potential annual evaporation ranges between 2800 and 3200mm per year with few pockets lying at 2600 and at 3400mm zones. Therefore, after exporting the attribute table of the evaporation map output in Figure 3-5, weighted mean annual potential evaporation on the Otjozondjupa is 3000mm. This equates to a lumped average daily potential evaporation rate of approximately 8.22mm. The average daily potential evaporation was assumed to be the maximum daily evaporation acting upon the open canal. When this was scaled to a rate of evaporation per second. It resulted in an evaporation rate of approximately 9.5×10^{-8}m/s.

3.9 Data analysis

3.9.1 Flow simulation and analysis of present canal hydraulic performance

After the HEC-RAS model 5.0 was set-up and made ready to perform a water surface profile simulation with the incorporation of flow and channel parameters.

The hydraulics of the open canal and the inverted siphons were evaluated by using the run analysis functionality of HEC-RAS 5.0. The hydraulic condition and behaviour of the canal system was evaluated based on calibration of Manning's n-values. This involved using all the observed discharge and water depth values as inputs for running simulations in HEC-RAS model. This was followed by iteratively process of finding the Manning's roughness coefficients that produced the best fit between observed and modelled discharge and stage hydrographs.

In order to prove the goodness of fit between observed and predicted discharge values, a correlation was performed and R^2-value of 95% was selected as the standard indicator of goodness of fit. Manning's roughness coefficients that were obtained from this process were taken as the effective roughness associated with the flow prevailing in the aqueduct. The effective Manning's roughness values obtained were presented in tabular format in terms of minimum, mean and maximum effective n-values for each reach of the canal system.

The effective Manning's coefficient was obtained as part of the HEC-RAS model results. The HEC-RAS model evaluates the Manning's friction equation for the roughness coefficients in a step-wise process for simulation of water surface profile at each cross-

section. To evaluate the change in roughness parameters, the Manning's n-values obtained based on the calibration procedure were compared to a Manning's n-value of 0.015 which is often the n-value for a newly laid surface in concrete channels [56]. This n-value was chosen because, the ENWC was laid with pre-fabricated appurtenances, therefore, the surface roughness at commissioning is assumed to have been very smooth. The comprehensive procedure for performing this flow evaluation in HEC-RAS model is contained in the User's manual [21].

Apart from determining the effective Manning's roughness coefficients, the flow simulation procedure was utilised for further evaluation and description of other channel hydraulic characteristics. Based on the prevailing boundary conditions, some of the hydraulic parameters calculated by HEC-RAS model include energy gradeline slope, flow velocities, flow area, wetted perimeter and Froude number. Flow analysis using HEC-RAS model is a holistic, step-wise and iterative process that include calculation of energy losses in the system. The total energy losses between any two cross-sections are taken as the sum of friction losses and contraction/expansion losses (equation 27) between those cross-sections.

The model calculates friction losses using a friction slope from the Manning's friction equation (Eq. 26) while the contraction/equation losses are computed as a product of the contraction/expansion coefficient and change in system velocity head (Eq. 27). The contraction/expansion coefficient is specified at the stage of inputting cross-sectional data and appropriate coefficients for different contraction and expansions are contained in literature [30]. This is how the water surface elevation profiles and other associated

hydraulic performance parameters were determined in order to show the hydraulic behaviour of the channel at present.

3.9.2 Simulating the water transportation maximum capacity

The HEC-RAS model was also used to evaluate the maximum water transportation capacity of the canal system between partial flumes 3 and 4 in its present hydraulic condition. The ability for the canal to accommodate increased flow was evaluated by holding the Manning's n roughness coefficients constant until when the discharge value associated with the minimum overflow hydrograph was obtained. During this procedure, the effective Manning's n-value obtained in the calibration procedure as specified in **Section 3.8.1**, was used in this step.

This was followed by scenario modelling based on iterative and discharge adjustment approach. As such, several different magnitudes of discharge were modeled and subsequently the model results were queried so as to evaluate the ability of the canal to carry and transmit those discharges. After several trials, it was decided to report on the model's ability to contain and transmit the stage hydrographs generated by the discharge magnitudes of 0.1, 0.3, 0.5, 0.7, 1, and 1.5 m^3/s. The largest discharge that produced a stage hydrograph that was contained by the canal systems up to a freeboard (F) of about 100mm was taken as the maximum capacity under present hydraulic conditions.

Once the maximum discharge was obtained, the associated boundary conditions at the upstream end, and hydraulic characteristics associated with the maximum Q, such as flow

velocity, Froude number, and head loss were summarised and reported in tabular form (see Table 4-1 and 4-2).

3.9.3 Sensitivity analysis of HEC-RAS model

A sensitivity analysis of changes to roughness parameters was performed in the following manner. Firstly, the effective Manning's n-values obtained based on the calibration and validation procedure described in **Section 3.8.1** were adjusted by 10% in both the positive and negative direction. Sequentially, HEC-RAS model was run to evaluate the impact of the changes in roughness parameters on discharge (Q) in the canal system. The comprehensive procedure for sensitivity analysis is contained in [21].

3.9.4 Leakage losses

Leakage losses along the canal sections, were evaluated using the inflow-outflow loss measurement method. In this case, the steady state conveyance losses were estimated as the difference in discharge per length of canal between the upstream and the downstream cross-section. The general principle of the inflow-outflow method is such that the magnitude of leakage losses is represented mathematically by the expression:

$$Q_L = Q_{in} - Q_{out} \qquad \text{(Eq. 32)}$$

On the other hand, the actual equation used for computing leakage losses from steady state flow is as flows:

$$Q_L = \frac{Q_u - Q_d}{L} \ \text{m}^3/\text{s/length (m)} \qquad \text{(Eq. 33)}$$

Where Q_L is the leakage losses (m^3/s), Q_u is the discharge at the upstream sampling point (m^3/s) and Q_d is the discharge at the downstream cross-section (m^3/s). The theoretical basis for using this method were the following:

1. The effect of friction losses on the magnitude of discharge was accounted for in the friction slope, so there was no need to factor friction losses into the inflow-outflow procedure and
2. The effect of evaporation losses can be approximated to zero given the difference in the time-step for flow gauging and distance between cross-sections were significantly small i.e. 15 to 30 minutes time differential between flow gauging on one cross-section to the next that are located between 300 to 500m from each other.

The said time step is not sufficiently long enough for any significant evaporation to occur and elicit water loss and reduction to the energy in the system between any two adjacent cross-sections.

3.9.5 Evaporation losses of water in transport

In this study, evaporation losses were evaluated by adopting the evaporation loss formula from the double-deck surface layer (DSAL) model. This model utilises an evaporation loss formula that is specifically adapted for estimating evaporation from water in transport (discharge). Most evaporation loss formula are more suitable for estimating evaporation over a stagnant body water like a pond or lake. As such, total evaporation loss of water in transport through a canal was then approximated from the evaporation loss equation:

$$E_L = E\frac{TL}{Q}, \quad \text{in } m^3/\text{day} \qquad \text{(Eq. 34)}$$

where E_L is the evaporation loss, E is the average daily rate of evaporation [28].

3.10 Research Ethics

In order to observe research ethics, other researchers' work that are paraphrased or quoted were properly acknowledged and credited, unless they are common knowledge. Most importantly, the research does not involve animal experimentation or human participants. Formal permission to conduct research on the NamWater canal was officially granted before any work was commenced.

4. RESULTS

4.1 Hydraulic behaviour of the canal

4.1.1 Elevation of the water surface profiles in the canal

The shape of the predicted water surface elevation profile of flow in the canal system and associated level of agreement between predicted and observed water surface profile is shown in Figure 4-1.

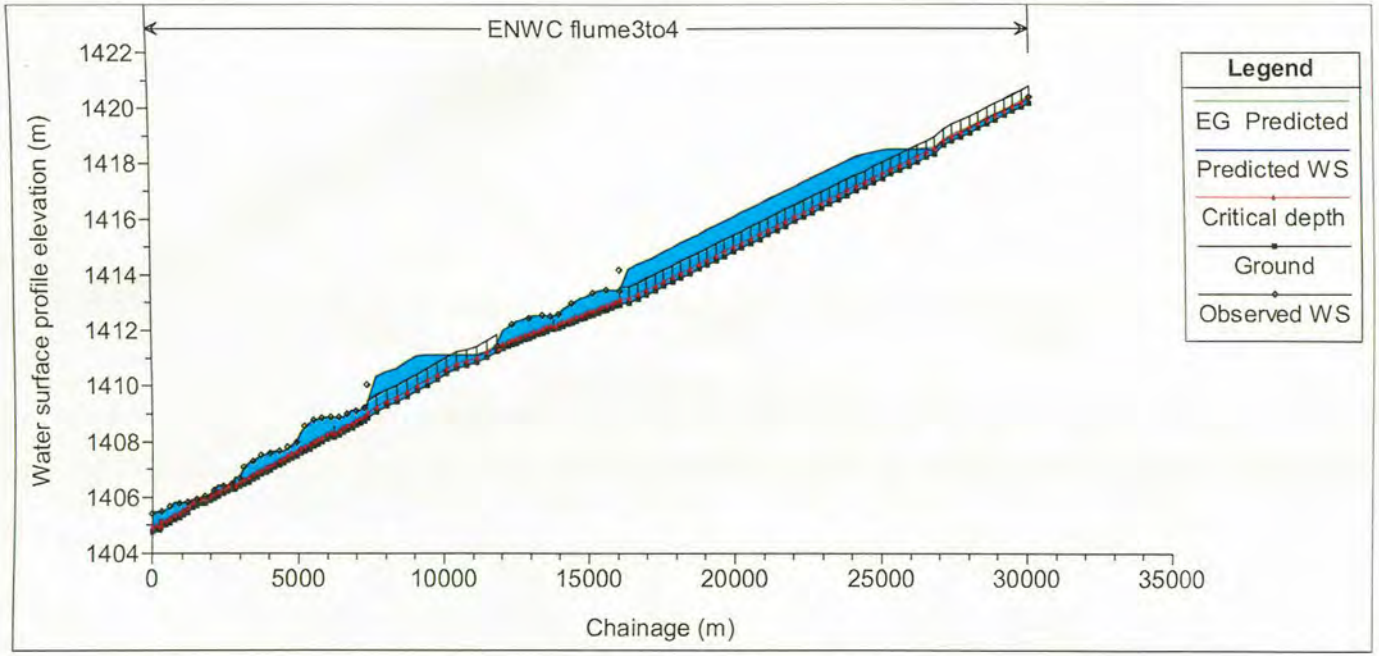

Figure 4-1 Predicted versus observed water surface elevation profile

To further indicate the extent of agreement between observed and predicted stage hydrograph of flow in the canal system, a zoomed-in graphic representation of the water surface elevation profiles is shown in Figure 4-2.

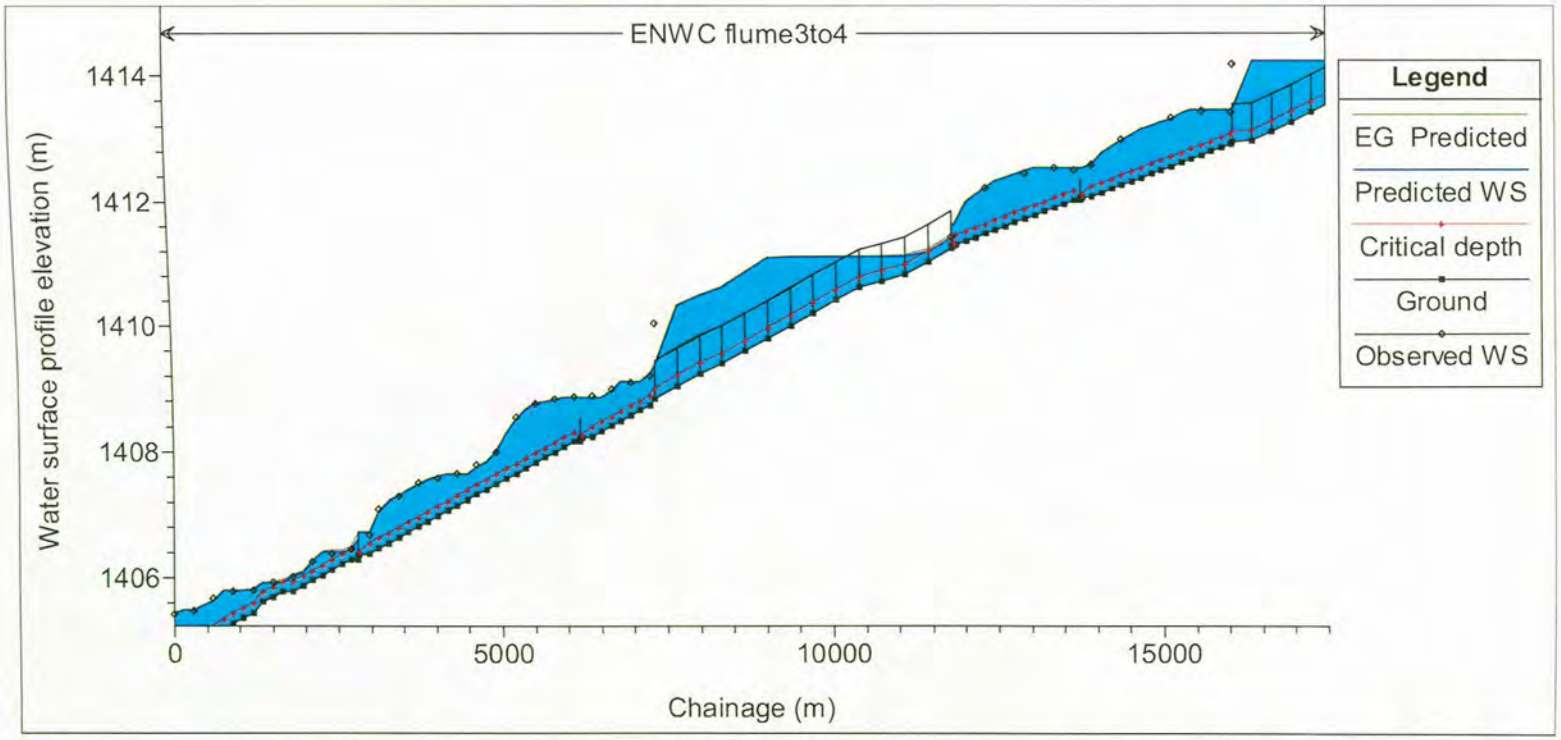

Figure 4-2 Predicted versus Observed water surface elevation profile (zoomed in to show greater agreement)

The scatter plot of the observed versus the predicted stage hydrograph associated with flow in the canal exhibits a higher agreement with an R^2-value of 0.997 obtained from 69 observed measurements along the study area as seen in Figure 4-3.

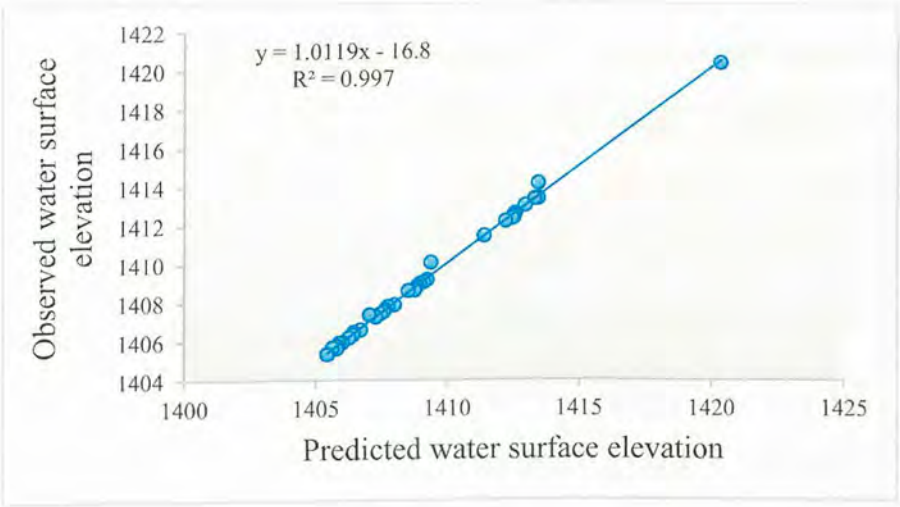

Figure 4-3 scatter plot of the observed against predicted water surface elevations

4.1.1 Flow velocity profile in the canal

The velocity profile for the predicted flow condition in the canal system is presented in Figure 4-4

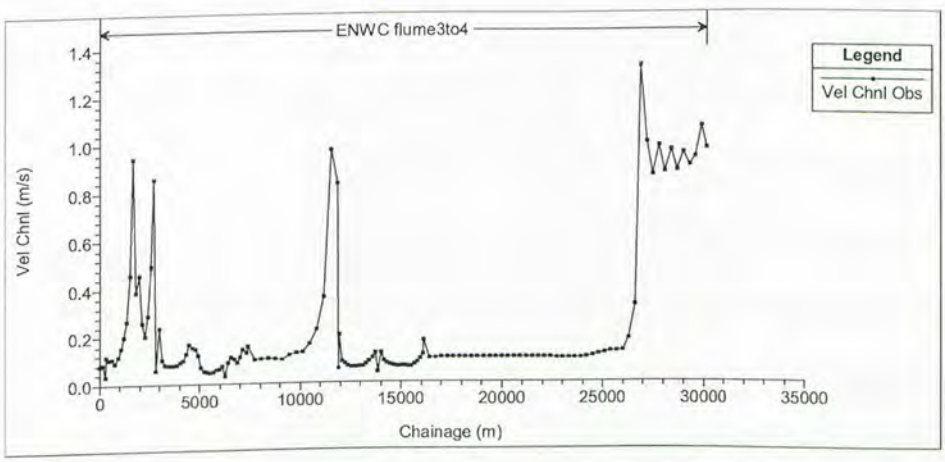

Figure 4-4 Predicted velocity profile for normal flow regime along channel chainage

4.1.2 Hydraulic characteristics of flow and calibrated Manning's n-values

Hydraulic properties associated with flow in canal system are shown in Table 4-1.

Table 4-1 Summary of calibrated Manning's n-values and hydraulic parameters

Hydraulic parameter		**Canal 1**	**Canal 2**	**Siphon 1**	**Siphon 2**
Effective Manning's n value	Min	0.001	0.001	0.003	0.005
	Mean	0.099	0.124	0.028	0.038
	Max	0.180	0.150	0.085	0.085
Energy slope (m/m)	Min	0.00000	0.00000	0.00000	0.00000
	Mean	0.00068	0.00108	0.00101	0.00099
	Max	0.00319	0.02026	0.00913	0.02427
Flow velocity (m/s)	Min	0.03	0.04	0.10	0.10
	Mean	0.17	0.08	0.26	0.33
	Max	0.94	0.20	0.98	1.32
Head loss gradient (m/km)	Total	0.62	0.43	0.51	0.50
Contraction and Expansion losses (m)	Total	0.0000	0.0000	0.0000	0.0000
Froude Number	Min	0.01	0.02	0.03	0.03
	Mean	0.12	0.04	0.19	0.28
	Max	1.02	0.13	0.99	1.52
Reynolds number	Min	53711.19	45390.23	59655.90	45406.76
	Mean	139783.8	134484.0	111108.9	134696.1
	Max	294911.3	337617.5	168103.1	373231.0

4.1.4 Graphic representation of the water surface elevation profile in open canal and lidded cross-section

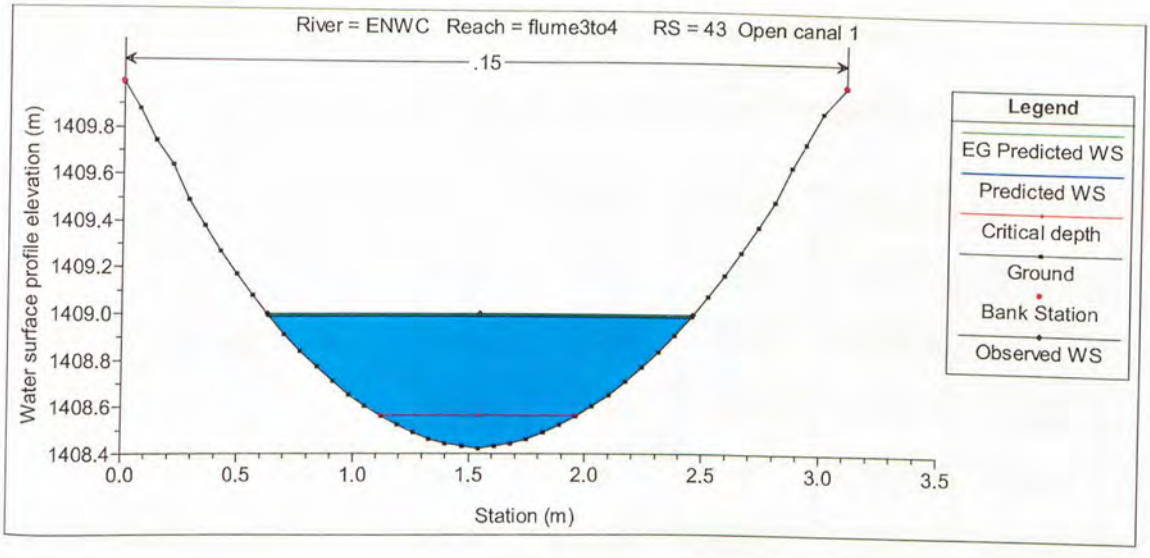

Figure 4-5 Predicted versus observed water surface profile at cross-section number 43

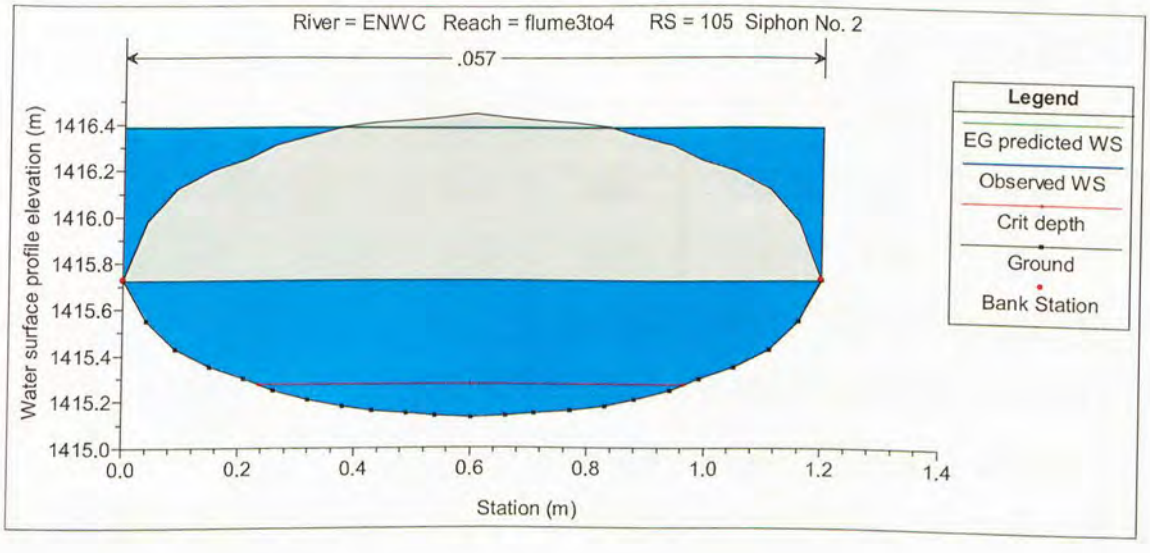

Figure 4-6 Water surface profile in a lidded cross-section

Figures 4-4 and 4-5 shows the general water surface profile in the open canal at cross-section number 43 and in the inverted siphon at cross-section 105. These figures also

exhibit the effective Manning's roughness coefficient values associated with predicted water surface elevation profiles.

4.2 Maximum water transportation capacity of the canal system

Table 4-2 Hydraulic characteristics for the maximum canal transportation capacity

Hydraulic parameter		**Canal 1**	**Canal 2**	**Siphon 1**	**Siphon 2**
Weighted Manning's n value	Min	0.001	0.001	0.003	0.005
	Mean	0.099	0.124	0.027846	0.038
	Max	0.180	0.150	0.085	0.085
Energy slope (m/m)	Min	0	0	0.00001	0.00003
	Mean	0.00062	0.00071	0.00026	0.00043
	Max	0.0053	0.00833	0.00118	0.00085
Flow velocity (m/s)	Min	0.06	0.07	0.15	0.17
	Mean	0.19	0.12	0.3	0.41
	Max	0.66	0.22	0.54	1.41
Head loss gradient (m/km)	Total	0.50	0.48	0.53	0.46
Froude number	Mean	0.08	0.04	0.08	0.2
Reynolds number	Min	193843.3	199043.5	137511.6	142977.3
	Mean	343646.5	285825.2	207934.1	323336.9
	Max	647211.2	401005	294000.4	945173.5
Estimated Maximum Capacity Discharge (Q) (m^3/s)	Max	0.5			

4.2.1 Water surface elevation profile for the maximum discharge

Figure 4-7 shows the shape of the water surface elevation profile of the flow representing the maximum transportation capacity of the canal system under its current hydraulic condition while the associated flow velocity profile is shown in Figure 4-8.

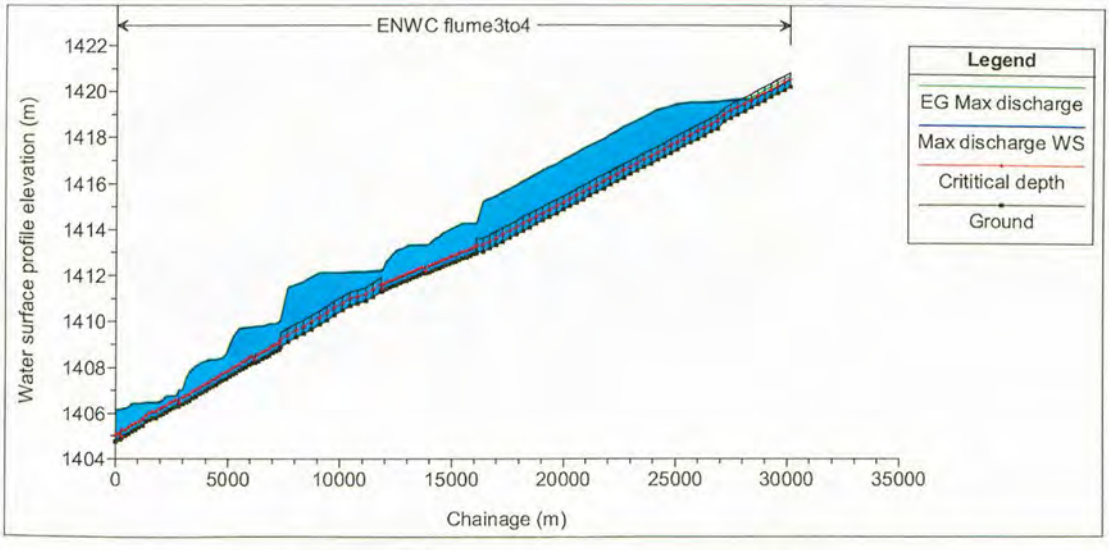

Figure 4-7 Water surface elevation profile for the maximum discharge

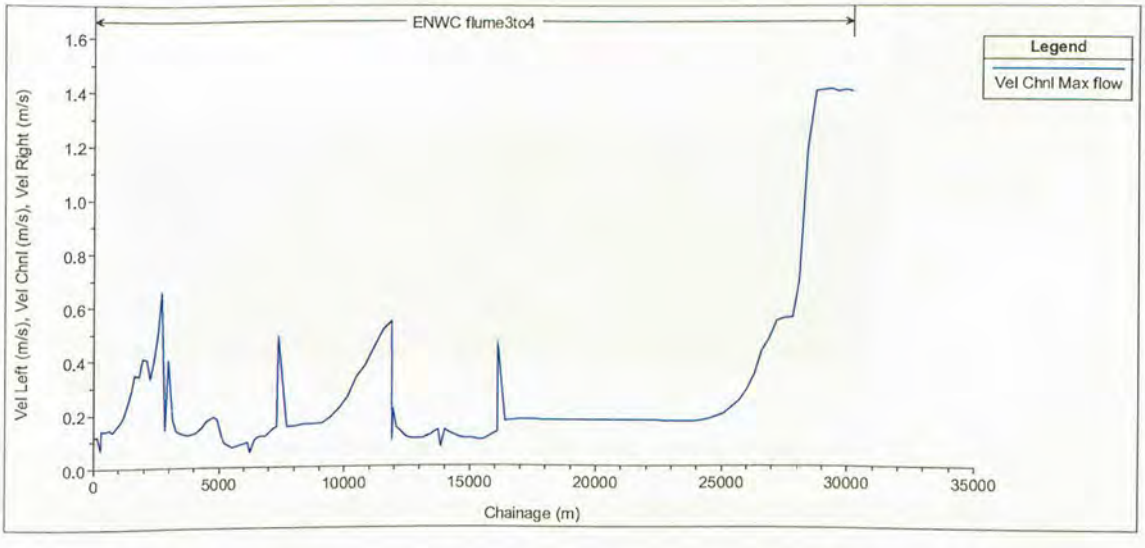

Figure 4-8 Predicted maximum discharge velocity graph along the channel chainage

4.2.2 Water surface profile at the lidded cross-section and inline structure

Graphic representation of the stage hydrograph of maximum at the lidded cross-section and flow over the long crested weir is shown in Figures 4-9 and 4-10.

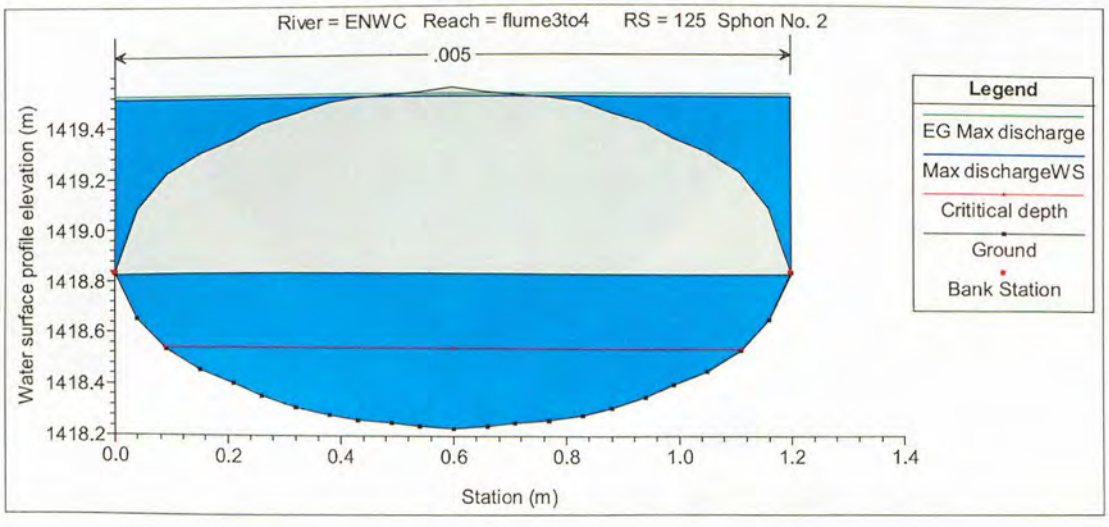

Figure 4-9 HEC-RAS cross-section with lid

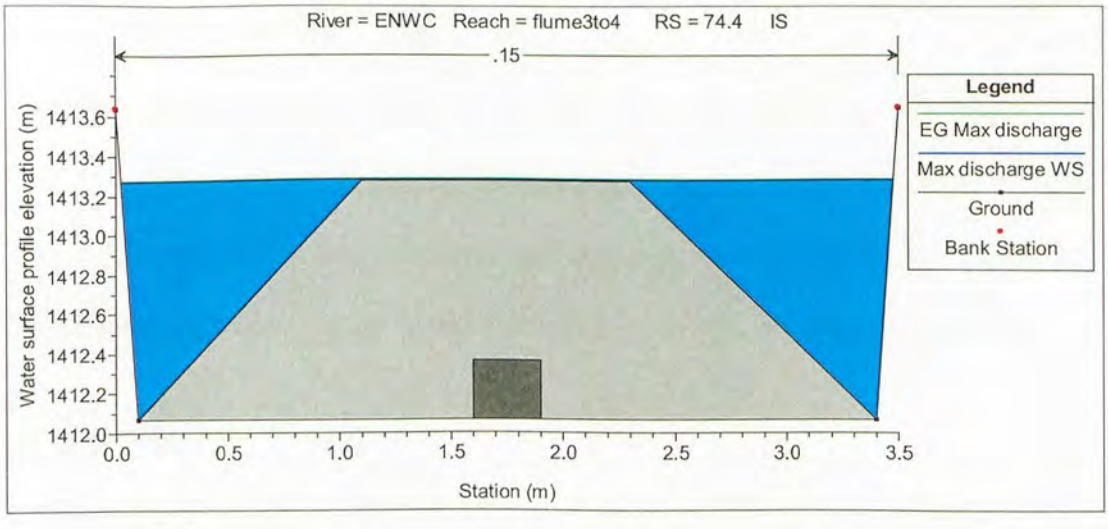

Figure 4-10 Flow over the cross-section with inline structure (long crested weir)

The graphic representation of the water surface elevation profile of maximum transportable discharge at the cross-section located at river station number 34 in Canal 1 is shown in Figure 4-11.

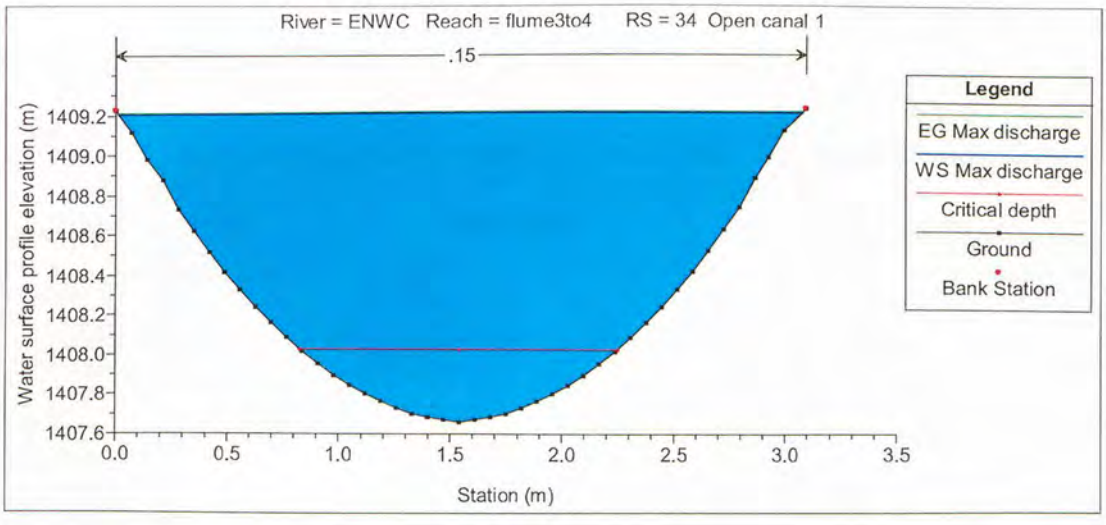

Figure 4-11 Cross-section on Canal 1, showing the water surface elevation profile of maximum discharge

4.3 Sensitivity analysis

The water surface elevation profile from a sensitivity analysis is not evidently different from the water surface elevation profiles for normal flow regimes presented in Figure 4-11. Also, a sensitivity analysis on the maximum transportation capacity did not yield a discernibly different graphic representation from the one reported in Figure 4-8.

4.4 Estimation of leakage and evaporation losses

Leakage and evaporation losses in the canal system that are associated with the present flow conditions, operation and state of maintenance are presented in the Tables 4.2 and 4-3. These losses are expressed both as the total discharge lost over the length of the

canal reach and as a percentage of the inflow discharge at the start of each channel reach type of the canal system

4.4.1 Leakage losses

Table 4-3 Summary of leakage losses

Channel	Total leakage loss (m^3/s)	Leakage loss (% of discharge)	Leakage loss (m^3/s per km)
Canal 1	0.010	25	0.0014
Canal 2	0.004	9.1	0.001
Siphon 1	0.010	20	0.0024
Siphon 2	0.018	25.7	0.0013

Figure 4-12 Hydraulic conditions of the canal

4.4.2 The evaporation losses in the open canal

Table 4-4 Summary of channel parameters and evaporation losses

Parameter	Channel reach	
	Canal 1	**Canal 2**
Total Channel Length (m)	7122	4180
Average topwidth of wetted cross-sectional area (m)	2.43	2.22
Flow length at each channel cross-section (m)	1	1
Average discharge in the channel (m^3/s)	0.035	0.042
Rate of evaporation (10^{-8} ms^{-1})	9.51	9.51
Minimum evaporation loss (% of discharge)	0.012	0.012
Average evaporation loss (% of discharge)	0.018	0.014
Maximum evaporation loss (% of discharge)	0.026	0.017

5. DISCUSSION OF RESULTS

5.1 Hydraulic behaviour of the canal

The hydraulic behaviour of the Eastern National Water Carrier between flumes 3 and 4 was evaluated based on the HEC-RAS model calibration procedure. As it is common that change in channel surface roughness often occurs in dissimilar manner and rate, at various channel reaches and different cross-section locations. A summary of effective Manning's roughness coefficients presented in Table 4.1, indicates that the average Manning's roughness coefficients (n) of 0.099, 0.124, 0.028 and 0.038 were respectively found in the four sections of the canal system i.e. Canal 1 and 2, and Siphon 1 and 2. On the other hand, the minimum n-values in these four sections of the aqueduct were found to range between 0.001 and 0.005. These results confirm that essentially different roughness conditions were present within the canal reach between flumes 3 and 4.

It was noticed that, the Manning's roughness coefficients obtained in this study seems to be comparatively higher than the values commonly reported for lined canals. However, whilst the roughness coefficients found during the calibration procedure seem to be abnormally higher, the graphic representation of the trend between observed and the predicted water surface profile elevations and discharges exhibited a good agreement as seen from Figures 4-1 to 4-3. As such, these results fairly represents the hydraulic state of the Eastern National Water Carrier between flumes 3 and 4 for the flow conditions at the time of the sampling.

This is supported by an R^2-value of 0.997 found during a trend analysis of 69 measurements taken over the length of the open canal sections. This indicates that very high correlation existed between observed and predicted stage and discharge hydrographs as visualised in Figure 4-3. While generally, a good agreement was observed between observed and predicted stage hydrograph, there were two points of highly distinct disagreement as indicated in the models results presented in Figure 4-1 to 4.3. This disagreement is attributed to a rapid change in cross-section size at the inverted siphon outlet structures. The size of the cross-section drastically change at those locations, from a 1.2m siphon diameter to an open canal of a topwidth of 3.1m over a chainage of few metres.

In order to perform a grading of the hydraulic performance and condition of the canal between flumes 3 and 4. A Manning's roughness coefficient $n = 0.012$ was selected as a benchmark for concrete lined aqueducts that have sound hydraulic performance and are generally in good hydraulic condition. Given that mean Manning's roughness coefficients $n = 0.099$, 0.124, 0.028 and 0.038 were found in the different sections of the open canal and inverted siphons, it can be said that the hydraulic performance and state of the ENWC reach from flumes 3 to 4 is not optimum. Also, when compared to the hydraulic performance and condition of lined concrete canals of similar design, the canal reach between flumes 3 to 4 appears to be of very bad hydraulic condition. This is supported by results found in similar studies i.e. a study done in the Mwea District of Kenya, found an average effective Manning's n-value of 0.023 for aging concrete lined irrigation canal [46] operated in tropical climatic conditions, while for circular

inverted siphons operated for over 30 years on the East Branch of the California Aqueduct, Manning's n-values in the range of 0.013 were found [47].

For canals in bad hydraulic condition i.e., those overlain with coarse sand sediment or overgrown with vegetation, it has been reported that such conditions can exhibit effective n-values of up to a maximum range of 0.070 [57] even though they are concrete lined. However, even when compared to such poor condition canals, the general hydraulic state of the canal reach between flumes 3 and 4, as described by the effective Manning's roughness coefficients as found in this study, was extremely poor condition for a concrete lined canal.

Regarding the condition of flow in the canal system, it can be said that flow regime was typically turbulent and subcritical. The minimum Reynolds number obtained over the entire canal chainage was Re = 45390.23 while mean Froude number calculated ranged between Fr = 0.04 and 0.28. The results found, support the observation that flow regime was generally turbulent and subcritical. However, certain sections in the canal were observed to have supercritical flow as demonstrated by the presence of Froude's number ranging between Fr = 1.02 and 1.52. This was attributed to the influence of inline long crested weirs on the flow regimes prevailing in canal.

Although flow velocities greater than 1m/s were observed at some cross-sections, the mean flow velocities of V = 0.17, 0.08, 0.26 and 0.33m/s were detected for Canal 1 and 2, & Siphons 1 and 2 respectively as summarised in Table 4-1. Further, the total head loss gradient of 0.62, 0.43, 0.51 and 0.50 m/km were observed in the same canal reaches. The average head loss gradient over the length of the channel between flumes

3 and 4 was 0.515 m/km compared to the bed slope of 0.580 m/km. The two slopes should be the same, but the presence of long crested weirs which serve to greatly control the flow in the canal can be linked to the variation in the channel bed and head loss gradients.

5.2 Maximum water transportation capacity of the canal system

The procedure to evaluate the maximum discharge that can be transported by the canal system between flumes 3 and 4 under its present hydraulic state involved simulation of a wide range of discharge values. In the present hydraulic state, it was found that maximum capacity of the canal system between flumes 3 and 4 was approximately Q = 0.3 m^3/s because this discharge satisfied all the requirements while the various sections of the canal were able to transmit discharges ranging between Q = 0.3 and 0.7 m^3/s. The summary of hydraulic parameters associated with this maximum discharge is presented in Table 4-4. While the water surface elevation profiles together with the graphic representation of how each different cross-section can accommodate the associated stage hydrograph are shown in Figures 4-7 to 4-11.

The stage hydrograph produced due to the interaction of the channel roughness, geometry and discharge is well contained in the canal. However, Figure 4-11 shows that even though there was no overflow at cross-section located at river station number 34, the set requirement of 100mm freeboard was not met. Nevertheless, the discharge of Q = 0.3 m^3/s was found to be a good approximation of the maximum capacity of the canal systems considering an abnormally roughness coefficient n = 0.15 was described at this cross-section.

Adopting such very large Manning's n-values may be a consequence for compensating for possible blockages in the vicinity of the specified cross-section. It was observed that the actual maximum capacity of the ENWC system between flumes 3 and 4 can be increased in the order of four to fivefold through strategic operation and maintenance. Thus, ensuring that the roughness characteristics of the canal system are generally very good can guarantee greater hydraulic performance of the canal without any major structural modifications [46], [47], [57].

The flow conditions representing maximum discharge in the canal system was completely turbulent and subcritical. This is so because the minimum Reynolds number obtained over the entire canal chainage was Re = 137511.60, which is higher than the threshold for turbulent flow by many folds. On the other hand, the maximum Froude number calculated for all flow velocities was Fr = 0.99 which lies below the threshold for critical flow described by the Froude number Fr = 1. Therefore, at this level of discharge, the flow conditions remained completely subcritical over the entire stretch of the canal system. For Q-maximum, flow velocities of V = 0.19, 0.12, 0.30 and 0.41m/s were reported for Canal 1 and 2, & Siphons 1 and 2 respectively. The associated head losses were 0.500, 0.480, 0.530 and 0.460 m/km were observed in Canal 1 and 2, & Siphons 1 and 2 respectively. The average head loss gradient over the length of the channel between flumes 3 and 4 was found to be 0.469 m/km compared to the bed slope of 0.580 m/km. The two slopes should be the same, but the presence of long crested weirs which serve to greatly control the flow in the canal can be linked to the variation in the channel bed and head loss gradients.

5.3 Sensitivity analysis of Manning's roughness coefficients

Changes to the roughness parameters in HEC-RAS did not result in any discernable impact on discharge. A variation of the Manning's n-values by 10% in the canal system, did not elicit noticeably changes to the stage hydrograph of normal flow regime and did not seem to cause changes to the estimated maximum capacity of the aqueduct between flumes 3 and 4.

These results are not consistent with general trend of reported sensitivity analysis results reported globally. A study on the hydraulic performance of concrete-lined irrigation canals in the Mwea district of Kenya, found that increasing the effective Manning's roughness coefficients from 0.022 to 0.027 and from 0.015 to 0.016, which represents a percentage change 22.3 and 6.7% resulted in a reduction in the estimated maximum capacity of the aqueduct by 11.61 and 10.975 respectively. The flow carried in the canals was in the order of Q =5.7 and 9.9 m^3/s. In another study on calibration of n-values found that a 5% percent decrease in discharge resulted in approximately 6% increase in Manning's n-values while a 5% increase in discharge lowered the roughness coefficients by about 4% where the discharge Q = 56.92 m^3/s was carried in the canal system.

While others found a positive relationship between change in roughness parameters and the response of the stage hydrograph associated with discharge in their studies. It is also plausible that in some cases, a change in manning's n-values will not yield a significant hydraulic response. This is supported by some studies that found that the stage hydrograph of flows of a lesser magnitude is characteristically not highly

sensitive to changes in roughness coefficients [58]. As such, the greater the flow rate, the more sensitive the water depth is to changes to Manning's roughness coefficients.

5.4 Leakage and evaporation losses

Leakage losses were evaluated based on the inflow-outflow method. Table 4-2 shows the varying magnitudes by which discharge was decreased by leakage losses in both canal and siphon reaches between flumes 3 and 4. Total leakage losses of $Q_L = 0.018$, 0.010, 0.004 and $0.010 m^3/s$ were observed in the four particular channel reaches between flumes 3 and 4 i.e. Siphon, 2 and 1, & Canal 2 and 1 in that order. These leakage losses represent the respective equivalent of $Q_L = 0.0013$, 0.0024, 0.001 and $0.0014 m^3/s$ per km. This suggests that in terms of leakages per unit length of the channel reach, the highest losses occurred in Siphon 1 while the lowest losses occurred in Canal 2. Intermediate losses were observed in Canal 1 and Siphon 2.

When expressing leakage losses as a percentage, it can be said that the losses observed in Siphons 1 and 2 represent 20 and 29.0% of mean discharge $Q = 0.050$ and $0.062 m^3/s$ in those canal reaches respectively. On the other hand, approximately 25 and 9.1% of the mean discharge $Q = 0.04$ and $0.044 m^3/s$ was lost in Canal 1 and 2 respectively. These results indicate that in three different sections of the canal reach between flumes 3 and 4, the magnitude of leakage losses was of the order of 20% or more, of mean discharge in those sections.

Generally, leakages in lined canals occur as seepage due to the presence of breaches on the channel bed. However, based on physical observation of the canal system, the channel bed appeared generally stable and intact with only few minor cracks present

on some sections on the walls of the open canal. Figure 4-6 (a) and (b) shows severe blockages in two different siphons between flumes 4 and 5 and how sediment deposits have reduced the diameter of the outlet structures of those inverted siphons. It is important to note that the channel reach between flume 4 and 5 lies outside the area of interest in respect of this study. However, because this section was not operational and its channel bed was drying up during the field excursion. The section was subjected to visual inspection in order to gain more insight on the state of the overall canal system. Therefore, in this study it is assumed and suggested that a similar hydraulic state as seen Figure 4-6 (a) and (b) may exist in similar structures in the study area.

On the other hand, Figure 4-6 (c), shows the extent to which long stretches in Canal 2 has a channel bed that is overgrown with vegetation while part (d) shows evidence of breaches of channel bed on sections of both Canal 1 and 2. The largest proportion of leakage losses observed in this study occurred in the siphons. Therefore, it is envisaged that leakage losses in inverted siphons did not occur as direct seepage losses but were predominantly driven by blockages.

In addition, overarching actors for leakage losses in the canal section were thought to be both sediment blockages on road-crossings the open canal and vegetation growth. Since the inflow-outflow method measures leakage losses, it is argued in this study that these losses reported may represent a combination of both leakage, local and friction losses. This is the most plausible situation because considering the physical state of the canal system along the study area, actual leakages are envisaged to be largely negligible.

In terms of the evaporation losses, firstly the lumped average potential evaporation rate over the Otjozondjupa region and which was also the assumed effective rate of evaporation loss along the Eastern National Water Carrier was 9.5×10^{-8} ms^{-1}. It can be seen in Table 4-3 that, the magnitude of evaporation loss ranged between 0.012 and 0.026% of discharge in Canal 1 while in Canal 2 the evaporation loss was found to be of the order of 0.012 to 0.017% of the discharge flowing in the canal.

The mean evaporation loss at a given channel cross-section was found to be of the order of 0.018 and 0.014% of discharge for canal reach 1 and canal reach 2 respectively. For the flow rate of 0.035 to $0.044m^3/s$, this represents total evaporation losses of the magnitude ringing between 47 and $54m^3/day$. These results suggests that in terms of contribution to total head losses, evaporation losses represent a significantly smaller part compared to other losses. In this study very low evaporation losses were found compared to a study that applied similar methods which found evaporation loss to be of the order of 1% of discharge [28]. This was attributed to the presence of comparatively very low discharge in the canal under study.

6. CONCLUSIONS AND RECOMMENDATIONS

6.1 Conclusion

The present hydraulic state of the canal system between flumes 3 to 4 is generally in very bad condition as indicated by how large the calculated mean roughness coefficients were, when compared to the benchmark roughness coefficient of $n = 0.012$. In fact, the mean Manning's roughness coefficients in the canal system were three to tenfold above the benchmark condition. This was thought to be a result of operating the canal below optimum coupled with inadequate maintenance regimes. The canal is presently operated under very low flow regimes that promote sediment deposition and vegetation growth.

To understand the transportation capacity of the canal, the estimated maximum capacity of the canal system under present hydraulic conditions was found to me $Q =$ 0.3 m^3/s. However, it was found that for both normal flow and estimated maximum capacity flow regimes, the associated stage hydrograph did not exhibit any sensitivity or discernible response to changes in roughness when coefficients were varied by 10% threshold.

The largest leakages occurred in inverted siphons and therefore, it is concluded that the impact of blockages is larger than that of vegetation growth on flow resistance and driving leakage losses. It is also, thought that what is reported as leakage losses, may actually be lumped head losses comprised of both leakages, local and friction losses stemming of blockage and impact of vegetation bed on discharge. It is also concluded that evaporation losses were significantly smaller and accounted for a negligible

proportion of total head losses. Therefore, with respect to the objective of the study, aspect related to the hydraulic condition and roughness of the channel bed in the canal system is largely affected by vegetation growth and blockages due to how the canal is operated and maintenance regimes than from the effect of natural aging.

6.2 Recommendations

Flume 3 can only transmit flow received from the preceding sections of the canal system. Therefore, it is recommended that a full hydraulic modelling study should be performed in order to evaluate the hydraulic performance and maximum capacity of the entire ENWC.

It is recommended that the canal be operated under optimum flow into order to maintain flow regimes that do not encourage sediment deposition in inverted siphons and excessive growth of a vegetation bed in the open canal system. This will increase the sustainability of the infrastructure. However, if the canal continues to be operated in the same manner, then it is recommended that the canal system maintenance be improved through adoption of robust cleaning and rehabilitation strategies and programs.

7. REFERENCES

[1] Department of Water Affairs, "Eastern National Water Carrier: Omatako Dam to Sartorius von Bach Dam," Windhoek, 1984.

[2] J. A. J. Aisenbrey, R. B. Hayes, H. J. Warren, D. L. Winsett, and R. B. Young, "Design of small canal structures," Denver, 1978.

[3] S. J. Van Vuuren and M. Van Dijk, "Determination of the change in Hydraulic Capacity in Pipelines," Pretoria, 2012.

[4] K. Patel, "Mathematical model of open channel flow for estimating velocity distribution through different surface roughness and discharge," *Int. J. Adv. Eng. Technol.*, vol. 3, no. 1, pp. 252–253, 2012.

[5] P. K. Swamee, G. C. Mishra, and B. R. Chahar, "Design of minimum earthwork cost canal sections," *Water Resour. Manag.*, vol. 15, no. 1, pp. 17–30, 2001.

[6] F. C. Scobey, "Flow of water in irrigation and similar canals," *United States Dep. Agric. -- Tech. Bull.*, no. 652, p. 78 ST-Flow of water in irrigation and similar c, 1939.

[7] D. P. E. Bennett and R. E. I. T. Glaser, "Common pitfalls in hydraulic design of large diameter pipes: case studeies and good design practice," *ASCE*, pp. 961–971, 2011.

[8] N. Rott, "Note on the history of Reynolds Number," *Annu. Rev. Fluid Mech.*,

vol. 22, pp. 1–11, 1990.

[9] J. Magnaudet and I. Eames, "The Motion of High-Reynolds-Number Bubbles in Inhomogeneous Flows," *Annu. Rev. Fluid Mech.*, vol. 32, no. 1, pp. 659–708, 2000.

[10] D. A. Savić, R. Casey, and Z. Kapelan, "Basic hydraulic principles," Waterbury, 2011.

[11] T. R. A.- Husseini, "Optimum hydraulic design for inverted siphon," *Al-Qadisiya J. Eng. Sci.*, vol. 1, no. 1, pp. 46–59, 2008.

[12] J. Fenton, "Open Channel Hydraulics 30.1," *Eng. Hydraul. Hydrol.*, pp. 421–316, 2005.

[13] B. H. E. Jobson and D. C. Froehlich, "Basic hydraulic principles of open channel flow, U . S . Geological Survey Dallas L . Peck , Director," Reston, 1988.

[14] D. . Tsombe, "Modelling fluid flow in open channel with circular cross-section," Jomo Kenyatta University of Agriculture and Technology, 2011.

[15] B. R. Chahar, "Optimal Design of Parabolic Canal Section," *J. Irrig. Drain. Eng.*, pp. 546–554, 2005.

[16] R. M. Mwiya, "Parabolic Channel Design," *Int. J. Sci. Eng. Res.*, vol. 4, no. 4, pp. 804–809, 2013.

[17] A. . Ghumman, M. . Khan, and M. . Khan, "Integration of drainage, water

quality and flood management in rural, Urban and lowland areas," *Irrig. Drain.*, vol. 55, pp. 161–177, 2007.

[18] X. Litrico and V. Fromion, "Smplified Modeling of Irigation Canals for Controller Design," *J. Irrig. Drain. Eng.*, vol. 130, no. 5, pp. 366–372, 2004.

[19] A. Sole and G. Zuccaro, "Comparison between open channel flow models in natural rivers," *Trans. Ecol. Environ.*, vol. 60, 2003.

[20] X. Liu, "Open Channel hydraulics: From then to now and beyond," *Handb. Environ. Eng.*, vol. 15, pp. 127–156, 2014.

[21] USACE, "HEC-RAS River Analysis System - Hydraulic Reference Manual, Version 5.0." U.S Army Corps of Engineers, Davis, p. 547, 2016.

[22] F. Bouchut, A. Mangeney-Castelnau, B. Perthame, and J. P. Vilotte, "A new model of Saint Venant and Savage–Hutter type for gravity driven shallow water flow," *Acad. des Sci.*, pp. 531–536, 2003.

[23] G. Akbari and B. Firoozi, "Implicit and Explicit Numerical Solution of Saint-Venent Equations for Simulating Flood Wave in Natural Rivers," in *5th National Congress on Civil Engineering*, 2010, pp. 2–8.

[24] J. de Halleux, C. Prieur, J.-M. Coron, B. D'Andrea-Novel, and G. Bastin, "Boundary feedback control in networks of open channels," *Automatica*, vol. 39, no. 8, pp. 1365–1376, 2003.

[25] J. D. Fenton, "Calculating Resistance to Flow in Open Channels," *Altern. Hydraul. Pap.*, no. 2, pp. 1–7, 2010.

[26] X. Y. Zhang and L. Wu, "Direct solutions for normal depths in curved irrigation canals," *J. Irrig. Drain. Eng.*, vol. 36, no. 1, pp. 9–13, 2014.

[27] A. F. Barton, "Friction , Roughness and Boundary Layer Characteristics of Freshwater Biofilms in Hydraulic Conduits," University of Tasmania, 2006.

[28] S. Liu, W. Wang, M. Mori, and T. Kobayashi, "Estimating the Evaporation from Irrigation Canals in Northwestern China Using the Double-Deck Surface Air Layer Model," *Adv. Meteorol.*, vol. 2016, p. 9, 2016.

[29] R. W. P. May, "Self-cleansing flow conditions for inverted siphons," Oxon, 2000.

[30] S. Earle and E. Krogh, "Geochemistry of Gabriola ' s groundwater," *Shale J.*, no. 7, pp. 35–42, 2004.

[31] W. B. White, "A brief history of karst hydrogeology: contributions of the NSS," *J. Cave Karst Stud.*, vol. 69, no. 1, pp. 13–26, 2007.

[32] L. Toombes and H. Chanson, "Numerical limitations of hydraulic models," in *10th Hydraulics Conference*, 2011, no. July, pp. 2322–2329.

[33] Y. Yi, C. Tang, Z. Yang, S. Zhang, and C. Zhang, "A One-dimensional hydrodynamic and water quality model for a water transfer project with multihydraulic structures," *Math. Probl. Eng.*, pp. 1–10, 2017.

[34] S. Alaghmand, R. Bin Abdullah, I. Abustan, and S. Eslamian, "Comparison between capabilities of HEC-RAS and MIKE11 hydraulic models in river flood risk modelling (a case study of Sungai Kayu Ara River basin,

Malaysia)," *Int. J. Hydrol. Sci. Technol.*, vol. 2, no. 3, p. 270, 2012.

[35] T. Z. Gichamo, I. Popescu, A. Jonoski, and D. Solomatine, "River cross-section extraction from the ASTER global DEM for flood modeling," *Environ. Model. Softw.*, vol. 31, pp. 37–46, 2012.

[36] G. W. Brunner, "Combined 1D and 2D Modeling with HEC-RAS," Davis, 2014.

[37] W. E. Fleenor and M. Jensen, "Evaluation of Numerical Models: HEC-RAS and DHI-MIKE 11," *J. Hydraul. Eng.*, pp. 1–15, 2003.

[38] L. Toombes and H. Chanson, "Numerical Limitations of Hydraulic Models," in *10th Hydraulics conference*, 2011, no. July, pp. 2322–2329.

[39] S. Li, Z. J.M, X. W.L, Y. . Wang, Y. Peng, L. J.N, X. . He, and P. Li, "Sensitivity analysis of parameters in HEC-RAS software," *Appl. Mech. Mater.*, vol. 641–642, pp. 201–204, 2014.

[40] B. Achour and M. Khattaoui, "Computation of Normal and Critical Depths in Parabolic Cross Sections," *Open Civ. Eng. J.*, vol. 2, pp. 9–14, 2008.

[41] P. Sclafani, "Methodology for predicting maximum velocity and shear stress in a snuous channel with bendway weirs using 1-D HEC-RAS modelling results," Colorado State University, 201AD.

[42] F. Pappenberger, P. Matgen, K. J. Beven, J. B. Henry, L. Pfister, and P. Fraipont, "Influence of uncertain boundary conditions and model structure on flood inundation predictions," *Adv. Water Resour.*, vol. 29, pp. 1430–1449, 2006.

[43] A. . Schmidt and B.CYen, "Stage-Discharge Relationship in Open Channels," *Hydrosystems Lab*, pp. 81–87, 2015.

[44] P. K. Parhi, R. N. Sankhua, and G. P. Roy, "Calibration of Channel Roughness for Mahanadi River, (India) Using HEC-RAS Model," *J. Water Resour. Prot.*, vol. 4, pp. 847–850, 2012.

[45] L. Kadhim Hameed and S. Tawfeek Ali, "Estimating of manning's roughness coefficient for Hilla river through calibration using HEC-RAS model," *Jordan J. Civ. Eng.*, vol. 7, no. 1, pp. 44–53, 2013.

[46] I. J. Serede, B. M. Mutua, and J. M. Raude, "A review for hydraulic analysis of irrigation canals using HEC-RAS model : A case study of Mwea irrigation scheme , Kenya," *Hydrology*, vol. 2, no. 1, pp. 1–5, 2014.

[47] M. Jensen, I. Tod, and J. Devries, "Application of RAS to the East Branch of the California Aqueduct," *USCID*, pp. 607–616, 2004.

[48] F. E. Hicks and T. Peacock, "Suitability of HEC-RAS for Flood Forecasting," *Can. Water Resour. J.*, pp. 159–174, 2005.

[49] P. Rao and T. Hromadka, "Numerical modeling of rapidly varying flows using HEC-RAS and WSPG models," *Springerplus*, vol. 2016, no. 5, p. 662, 2016.

[50] Y. Yi, C. Tang, Z. Yang, S. Zhang, and C. Zhang, "A One-Dimensional Hydrodynamic and Water Quality Model for a Water Transfer Project with Multihydraulic Structures," *Hindawi*, pp. 87–96, 2017.

[51] K. T. Lee, Y.-H. Ho, and Y.-J. Chyan, "Bridge Blockage and Overbank Flow Simulations Using HEC–RAS in the Keelung River during the 2001 Nari Typhoon," *J. Hydraul. Eng.*, pp. 319–323, 2006.

[52] NSA, "Namibia 2011 population and housing census preliminary results," Windhoek, 2011.

[53] M. O. Katuuo, "The study to investigate water provision by Okakarara Town Council," University of Namibia, 2014.

[54] N. Jurgens, D. . Haarmeyer, J. Luther-Mosebach, J. Dengler, M. Finckh, and Schmiedel, Eds., *Patterns at Local Scale: The BIOTA Observatories, Biodiversity in Southern Africa*. Windhoek: Klaus Hess Publishers, 2010.

[55] J. Mendelsohn, A. Jarvis, C. Roberts, and T. Robertson, *Atlas of Namibia*. Cape Town: David Philip Publishers, 2002.

[56] T. Lenhart, K. Eckhardt, N. Fohrer, and H. Frede, "Comparison of two different approaches of sensitivity analysis," *Phys. Chem. Earth*, vol. 27, pp. 645–654, 2002.

[57] B. J. V Phillips and S. Tadayon, "Selection of Manning ' s Roughness Coefficient for Natural and Constructed Vegetated and Non- Vegetated Channels , and Vegetation Maintenance Plan Guidelines for Vegetated

Channels in Central Arizona Scientic Investigations Report 2006 – 5108," South Boston, 2006.

[58] F. Pappenberger, K. Beven, M. Horritt, and S. Blazkova, "Uncertainty in the calibration of effective roughness parameters in HEC-RAS using inundation and downstream level observations," vol. 302, pp. 46–69, 2005.

APPENDICES

Appendix A: Google Maps insert of the Eastern National Water Carrier

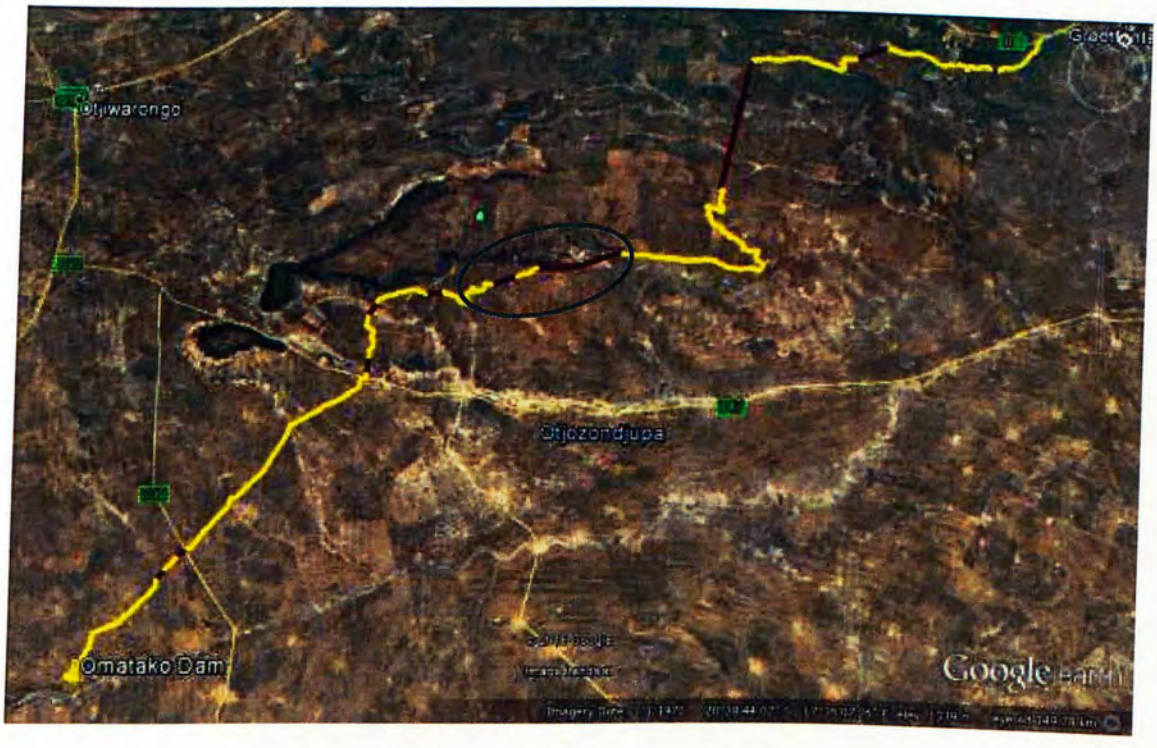

Figure A-1 Study area (Flume 3 to Flume 4) circled in black

Appendix B Canal geometry schematic with cross-section outline

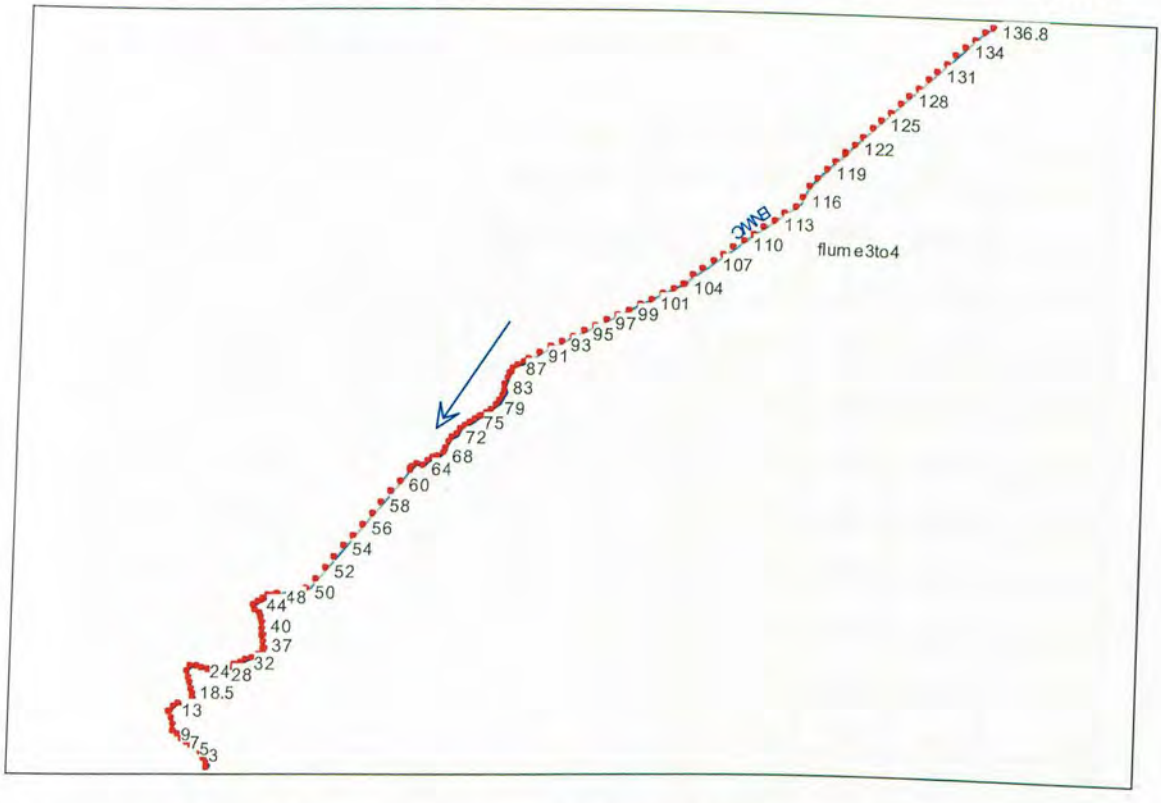

Figure B-1 Channel geometry with user-defined and interpolated cross-sections

Appendix C: Steady flow description

Table C-1 Flow data for scenarios for estimation canal maximum capacity

River	Reach	RS	M1	Max flow	M3	M4	M5	PF 6	PF 7
ENWC	flume3to4	136.8	0.1	0.3	0.5	0.7	1	1.5	2

The flow regimes used in the simulation of the maximum discharge or transportation capacity of the canal system in its present hydraulic state.

Appendix D

(a) Profile output table for observed flow

River Station #	Pro file	Q Total	Min Ch El	W.S. Elev	Crit W.S.	E.G. Elev	E.G. Slope	Vel Chnl	Flow Area	Top Width	Froude # Canal
		(m3/s)	(m)	(m)	(m)	(m)	(m/m)	(m/s)	(m2)	(m)	
136.8	Obs	0.07	1420.21	1420.38	1420.38	1420.43	0.000224	1.04	0.07	0.61	0.99
136	Obs	0.07	1420.05	1420.18	1420.22	1420.32	0.00082	1.65	0.04	0.52	1.84
135	Obs	0.07	1419.9	1420.04	1420.07	1420.13	0.000472	1.35	0.05	0.56	1.42
134	Obs	0.07	1419.74	1419.88	1419.91	1419.98	0.000545	1.42	0.05	0.55	1.52
133	Obs	0.07	1419.59	1419.73	1419.76	1419.83	0.000496	1.37	0.05	0.56	1.45
132	Obs	0.07	1419.43	1419.57	1419.6	1419.67	0.000519	1.4	0.05	0.56	1.48
131	Obs	0.07	1419.28	1419.42	1419.45	1419.52	0.000522	1.4	0.05	0.55	1.49
130	Obs	0.07	1419.12	1419.26	1419.3	1419.36	0.000519	1.4	0.05	0.56	1.48
129	Obs	0.07	1418.97	1419.11	1419.14	1419.21	0.000523	1.4	0.05	0.55	1.49
128	Obs	0.07	1418.81	1418.95	1418.99	1419.05	0.00052	1.4	0.05	0.56	1.48
127	Obs	0.07	1418.66	1418.8	1418.83	1418.9	0.00052	1.4	0.05	0.55	1.48
126	Obs	0.07	1418.36	1418.77	1418.53	1418.78	0.000006	0.28	0.25	0.93	0.17
125	Obs	0.07	1418.23	1418.77	1418.4	1418.77	0.000002	0.18	0.39	1.11	0.1
124	Obs	0.07	1418.07	1418.77	1418.24	1418.77	0.000031	0.15	0.46	0.15	0.06
123	Obs	0.07	1417.92	1418.76	1418.09	1418.76	0.000028	0.14	0.5	0.34	0.05
122	Obs	0.07	1417.76	1418.75	1417.93	1418.75	0.000192	0.13	0.56	0.52	0.04
121	Obs	0.07	1417.61	1418.7	1417.78	1418.7	0.000147	0.11	0.62	0.71	0.03
120	Obs	0.07	1417.45	1418.63	1417.62	1418.63	0.000407	0.1	0.69	1.01	0.03
119	Obs	0.07	1417.3	1418.49	1417.47	1418.49	0.000495	0.1	0.71	1.14	0.03
118	Obs	0.07	1417.14	1418.34	1417.31	1418.34	0.000522	0.1	0.72	1.16	0.03
117	Obs	0.07	1416.99	1418.18	1417.16	1418.18	0.000526	0.1	0.71	1.14	0.03
116	Obs	0.07	1416.83	1418.03	1417	1418.03	0.000492	0.1	0.72	1.16	0.03
115	Obs	0.07	1416.68	1417.89	1416.85	1417.89	0.000466	0.1	0.73	1.2	0.03
114	Obs	0.07	1416.52	1417.74	1416.69	1417.74	0.000518	0.09	0.74	1.2	0.03
113	Obs	0.07	1416.37	1417.58	1416.54	1417.58	0.000521	0.09	0.74	1.2	0.03

River Station #	Pro file	Q Total	Min Ch El	W.S. Elev	Crit W.S.	E.G. Elev	E.G. Slope	Vel Chnl	Flow Area	Top Width	Froude # Canal
112	Obs	0.07	1416.21	1417.43	1416.38	1417.43	0.000521	0.09	0.74	1.2	0.03
111	Obs	0.07	1416.06	1417.27	1416.23	1417.27	0.000528	0.1	0.74	1.2	0.03
110	Obs	0.07	1415.9	1417.11	1416.07	1417.11	0.000551	0.1	0.73	1.2	0.03
109	Obs	0.07	1415.75	1416.95	1415.92	1416.95	0.000518	0.1	0.72	1.18	0.03
108	Obs	0.07	1415.59	1416.79	1415.77	1416.79	0.000519	0.1	0.72	1.17	0.03
107	Obs	0.07	1415.44	1416.64	1415.61	1416.64	0.000477	0.1	0.73	1.2	0.03
106	Obs	0.07	1415.28	1416.49	1415.46	1416.49	0.000548	0.1	0.73	1.2	0.03
105	Obs	0.07	1415.13	1416.33	1415.3	1416.33	0.000511	0.1	0.72	1.2	0.03
104	Obs	0.07	1414.97	1416.18	1415.15	1416.18	0.000504	0.1	0.73	1.2	0.03
103	Obs	0.07	1414.82	1416.03	1414.99	1416.03	0.000486	0.1	0.74	1.2	0.03
102	Obs	0.07	1414.66	1415.88	1414.83	1415.88	0.000516	0.09	0.74	1.2	0.03
101	Obs	0.07	1414.51	1415.73	1414.68	1415.73	0.000517	0.09	0.74	1.2	0.03
100	Obs	0.07	1414.35	1415.57	1414.53	1415.57	0.000516	0.09	0.74	1.2	0.03
99	Obs	0.07	1414.2	1415.42	1414.37	1415.42	0.000517	0.09	0.74	1.2	0.03
98	Obs	0.07	1414.04	1415.26	1414.21	1415.26	0.000516	0.09	0.74	1.2	0.03
97	Obs	0.07	1413.89	1415.11	1414.06	1415.11	0.000515	0.09	0.74	1.2	0.03
96	Obs	0.07	1413.73	1414.95	1413.91	1414.95	0.000512	0.09	0.74	1.2	0.03
95	Obs	0.07	1413.58	1414.8	1413.75	1414.8	0.000504	0.09	0.75	1.2	0.03
94	Obs	0.07	1413.42	1414.65	1413.59	1414.65	0.000487	0.09	0.75	1.2	0.03
93	Obs	0.07	1413.27	1414.51	1413.44	1414.51	0.000449	0.09	0.77	1.2	0.03
92	Obs	0.07	1413.11	1414.37	1413.29	1414.37	0.000475	0.09	0.79	1.2	0.03
91	Obs	0.07	1412.98	1414.19	1413.15	1414.19	0.000807	0.1	0.73	1.2	0.03
90	Obs	0.07	1412.95	1413.46	1413.12	1413.46	0.03493	0.2	0.35	1.05	0.11
89	Obs	0.07	1412.93	1413.46		1413.46	0.000001	0.11	0.61	1.76	0.06
88	Obs	0.07	1412.87	1413.46		1413.46	0.000003	0.1	0.72	1.86	0.05
87	Obs	0.07	1412.81	1413.46		1413.46	0	0.08	0.83	1.95	0.04
86	Obs	0.07	1412.75	1413.46		1413.46	0.000005	0.07	0.95	2.05	0.03
85	Obs	0.07	1412.69	1413.46		1413.46	0.00033	0.07	1.07	2.13	0.03
84	Obs	0.07	1412.63	1413.4		1413.4	0.000472	0.07	1.08	2.14	0.03

River Station #	Pro file	Q Total	Min Ch El	W.S. Elev	Crit W.S.	E.G. Elev	E.G. Slope	Vel Chnl	Flow Area	Top Width	Froude # Canal
83	Obs	0.07	1412.57	1413.33		1413.33	0.00051	0.07	1.05	2.12	0.03
82	Obs	0.07	1412.51	1413.26		1413.26	0.000362	0.07	1.04	2.11	0.03
81	Obs	0.07	1412.45	1413.21		1413.21	0.000349	0.07	1.05	2.12	0.03
80	Obs	0.07	1412.39	1413.15		1413.15	0.000509	0.07	1.05	2.12	0.03
79	Obs	0.07	1412.33	1413.07		1413.07	0.000569	0.07	1.01	2.09	0.03
78	Obs	0.07	1412.27	1412.97		1412.97	0.000692	0.07	0.94	2.03	0.04
77	Obs	0.07	1412.21	1412.88		1412.88	0.000599	0.08	0.86	1.98	0.04
76	Obs	0.07	1412.15	1412.77		1412.77	0.000793	0.09	0.78	1.91	0.04
75	Obs	0.07	1412.09	1412.6		1412.6	0.001883	0.12	0.57	1.72	0.07
74.5	Obs	0.07	1412.06	1412.54	1412.1	1412.54	0.000163	0.04	1.59	3.36	0.02
74.4		Inl Struct									
74	Obs	0.07	1412.03	1412.54		1412.54	0	0.12	0.57	1.72	0.07
73	Obs	0.07	1411.97	1412.54		1412.54	0	0.1	0.68	1.83	0.05
72	Obs	0.07	1411.91	1412.54		1412.54	0	0.09	0.79	1.92	0.04
71	Obs	0.07	1411.85	1412.54		1412.54	0	0.08	0.91	2.01	0.04
70	Obs	0.07	1411.79	1412.54		1412.54	0.00037	0.07	1.03	2.1	0.03
69	Obs	0.07	1411.73	1412.48		1412.48	0.000359	0.07	1.04	2.11	0.03
68	Obs	0.07	1411.67	1412.43		1412.43	0.000344	0.07	1.06	2.12	0.03
67	Obs	0.07	1411.61	1412.38		1412.38	0.000326	0.06	1.08	2.14	0.03
66	Obs	0.07	1411.55	1412.32		1412.32	0.000464	0.06	1.08	2.14	0.03
65	Obs	0.07	1411.49	1412.22		1412.22	0.001138	0.07	0.99	2.08	0.03
64	Obs	0.07	1411.43	1412.1		1412.1	0.000586	0.08	0.87	1.98	0.04
63	Obs	0.07	1411.37	1412		1412	0.000754	0.09	0.79	1.92	0.04
62	Obs	0.07	1411.31	1411.68		1411.68	0.019916	0.2	0.35	1.45	0.13
61.5	Obs	0.07	1411.28	1411.64	1411.32	1411.64	0.000405	0.06	1.18	3.35	0.03
61.4		Inl Struct									
61	Obs	0.07	1411.25	1411.42	1411.42	1411.47	0.000059	1.05	0.07	0.6	1.01
60	Obs	0.07	1411.04	1411.15	1411.22	1411.37	0.007258	2.06	0.03	0.49	2.49

River Station #	Pro file	Q Total	Min Ch El	W.S. Elev	Crit W.S.	E.G. Elev	E.G. Slope	Vel Chnl	Flow Area	Top Width	Froude # Canal
59	Obs	0.07	1410.84	1411.04	1411.01	1411.07	0.000174	0.85	0.08	0.65	0.76
58	Obs	0.07	1410.73	1411.05	1410.9	1411.06	0.000011	0.4	0.18	0.83	0.27
57	Obs	0.07	1410.64	1411.06	1410.81	1411.06	0.000008	0.27	0.26	0.93	0.16
56	Obs	0.07	1410.43	1411.05	1410.61	1411.06	0.000013	0.15	0.45	0.03	0.06
55	Obs	0.07	1410.23	1411.05	1410.4	1411.05	0.000012	0.14	0.49	0.31	0.05
54	Obs	0.07	1410.03	1411.05	1410.2	1411.05	0.000011	0.12	0.58	0.58	0.04
53	Obs	0.07	1409.82	1411.04	1410	1411.04	0.000538	0.1	0.73	1.2	0.03
52	Obs	0.07	1409.62	1410.82	1409.8	1410.82	0.000749	0.1	0.72	1.18	0.03
51	Obs	0.07	1409.42	1410.62	1409.59	1410.62	0.000454	0.1	0.72	1.2	0.03
50	Obs	0.07	1409.27	1410.47	1409.44	1410.47	0.000408	0.1	0.73	1.2	0.03
49	Obs	0.07	1409.07	1410.26	1409.24	1410.26	0.000992	0.1	0.72	1.18	0.03
48	Obs	0.07	1408.86	1409.39	1409.04	1409.4	0.01508	0.19	0.37	1.09	0.1
47	Obs	0.07	1408.76	1409.26		1409.26	0.000696	0.13	0.54	1.69	0.07
46	Obs	0.07	1408.68	1409.14		1409.14	0.000978	0.15	0.48	1.62	0.09
45	Obs	0.07	1408.59	1409.14		1409.14	0	0.11	0.62	1.77	0.06
44	Obs	0.07	1408.51	1409.14		1409.14	0.000792	0.09	0.78	1.91	0.04
43	Obs	0.07	1408.42	1408.99		1408.99	0.001216	0.1	0.67	1.81	0.06
42	Obs	0.07	1408.34	1408.88		1408.89	0.00046	0.11	0.63	1.78	0.06
41	Obs	0.07	1408.25	1408.88		1408.88	0.000001	0.09	0.78	1.92	0.04
40.5	Obs	0.07	1408.23	1408.88	1408.27	1408.88	0.000009	0.03	2.19	3.38	0.01
40.4		Inl Struct									
40	Obs	0.07	1408.17	1408.88		1408.88	0	0.07	0.95	2.05	0.03
39	Obs	0.07	1408.08	1408.88		1408.88	0.000416	0.06	1.13	2.17	0.03
38	Obs	0.07	1408	1408.84		1408.84	0.000237	0.06	1.21	2.22	0.02
37	Obs	0.07	1407.91	1408.82		1408.82	0.000077	0.05	1.36	2.31	0.02
36	Obs	0.07	1407.83	1408.79		1408.79	0.000724	0.05	1.5	2.39	0.02
35	Obs	0.07	1407.74	1408.68		1408.68	0.00083	0.05	1.43	2.34	0.02
34	Obs	0.07	1407.66	1408.53		1408.53	0.001076	0.05	1.3	2.27	0.02
33	Obs	0.07	1407.57	1408.31		1408.31	0.00223	0.07	0.99	2.08	0.03

River Station #	Pro file	Q Total	Min Ch El	W.S. Elev	Crit W.S.	E.G. Elev	E.G. Slope	Vel Chnl	Flow Area	Top Width	Froude # Canal
32	Obs	0.07	1407.49	1408		1408	0.001859	0.12	0.57	1.72	0.07
31	Obs	0.07	1407.4	1407.86		1407.86	0.000601	0.15	0.47	1.61	0.09
30	Obs	0.07	1407.32	1407.76		1407.76	0.000654	0.15	0.46	1.59	0.09
29	Obs	0.07	1407.23	1407.65		1407.65	0.000856	0.17	0.41	1.54	0.1
28	Obs	0.07	1407.15	1407.65		1407.65	0.000002	0.13	0.55	1.7	0.07
27	Obs	0.07	1407.06	1407.65		1407.65	0.000343	0.1	0.7	1.84	0.05
26	Obs	0.07	1406.98	1407.61		1407.61	0.000258	0.09	0.78	1.91	0.05
25	Obs	0.07	1406.89	1407.56		1407.56	0.000403	0.08	0.85	1.97	0.04
24	Obs	0.07	1406.81	1407.49		1407.49	0.000577	0.08	0.88	1.99	0.04
23	Obs	0.07	1406.72	1407.4		1407.4	0.000583	0.08	0.87	1.99	0.04
22	Obs	0.07	1406.64	1407.31		1407.31	0.000592	0.08	0.87	1.98	0.04
21	Obs	0.07	1406.55	1407.22		1407.22	0.000612	0.08	0.86	1.98	0.04
20	Obs	0.07	1406.47	1407.05		1407.05	0.003193	0.1	0.68	1.83	0.05
19	Obs	0.07	1406.38	1406.72		1406.72	0.00153	0.24	0.3	1.37	0.16
18.5	Obs	0.07	1406.37	1406.72	1406.41	1406.72	0	0.06	1.18	3.35	0.03
18.4		Inl Struct									
18	Obs	0.07	1406.3	1406.45	1406.44	1406.49	0.000797	0.86	0.08	0.87	0.9
17	Obs	0.07	1406.21	1406.42		1406.44	0.000171	0.49	0.14	1.06	0.43
16	Obs	0.07	1406.13	1406.42		1406.43	0.000028	0.29	0.24	1.27	0.21
15	Obs	0.07	1406.04	1406.41		1406.42	0.001032	0.2	0.34	1.44	0.13
14	Obs	0.07	1405.96	1406.28		1406.28	0.000821	0.26	0.27	1.32	0.18
13	Obs	0.07	1405.87	1406.09		1406.11	0.001744	0.46	0.15	1.09	0.39
12	Obs	0.07	1405.79	1406.03	1405.93	1406.04	0.000186	0.39	0.18	1.16	0.31
11	Obs	0.07	1405.79	1405.93	1405.93	1405.97	0.002242	0.94	0.07	0.84	1.02
10	Obs	0.07	1405.7	1405.92	1405.85	1405.94	0	0.46	0.15	1.09	0.39
9	Obs	0.07	1405.62	1405.93		1405.94	0.000443	0.27	0.26	1.31	0.19
8	Obs	0.07	1405.45	1405.82		1405.82	0.001386	0.2	0.35	1.45	0.13
7	Obs	0.07	1405.36	1405.81		1405.81	0.000035	0.15	0.45	1.59	0.09
6	Obs	0.07	1405.28	1405.81		1405.81	0	0.12	0.6	1.75	0.06

River Station #	Pro file	Q Total	Min Ch El	W.S. Elev	Crit W.S.	E.G. Elev	E.G. Slope	Vel Chnl	Flow Area	Top Width	Froude # Canal
5	Obs	0.07	1405.19	1405.81		1405.81	0.000874	0.09	0.75	1.89	0.05
4	Obs	0.07	1405.09	1405.65		1405.65	0.001369	0.11	0.64	1.79	0.06
3	Obs	0.07	1405	1405.56		1405.56	0.000324	0.11	0.65	1.8	0.06
2	Obs	0.07	1404.98	1405.5		1405.5	0.000433	0.12	0.59	1.73	0.07
1.5	Obs	0.07	1404.89	1405.5	1404.93	1405.5	0.000019	0.03	2.03	3.38	0.01
1.4		Inl Struct									
1	Obs	0.07	1404.85	1405.5		1405.5	0.000246	0.09	0.82	1.95	0.04
0	Obs	0.07	1404.77	1405.45	1404.91	1405.45	0.00058	0.08	0.87	1.99	0.04

(b) Table D-2 Profile output for maxim flow capacity

River Station	Profile	Q Total	Min Ch El	W.S. Elev	Crit W.S.	E.G. Elev	E.G. Slope	Vel Chnl	Flow Area	Top Width	Froude # Canal
		(m3/s)	(m)	(m)	(m)	(m)	(m/m)	(m/s)	(m2)	(m)	
136.8	Max flow	0.3	1420.21	1420.52	1420.52	1420.62	0.000513	1.4	0.21	1.03	0.98
136	Max flow	0.3	1420.05	1420.36	1420.36	1420.46	0.000523	1.4	0.21	1.03	0.98
135	Max flow	0.3	1419.9	1420.21	1420.21	1420.31	0.000507	1.4	0.21	1.03	0.97
134	Max flow	0.3	1419.74	1420.05	1420.05	1420.15	0.000525	1.41	0.21	1.03	0.99
133	Max flow	0.3	1419.59	1419.9	1419.89	1420	0.000513	1.4	0.21	1.02	0.98
132	Max flow	0.3	1419.43	1419.74	1419.74	1419.84	0.000518	1.4	0.21	1.03	0.98
131	Max flow	0.3	1419.28	1419.62	1419.59	1419.7	0.000317	1.18	0.25	1.06	0.77
130	Max flow	0.3	1419.12	1419.63	1419.43	1419.65	0.000073	0.69	0.43	1.16	0.36
129	Max flow	0.3	1418.97	1419.62	1419.27	1419.63	0.000081	0.55	0.54	0.02	0.22
128	Max flow	0.3	1418.81	1419.59	1419.12	1419.61	0.000087	0.55	0.55	0.06	0.2
127	Max flow	0.3	1418.66	1419.56	1418.97	1419.58	0.000091	0.54	0.56	0.12	0.18
126	Max flow	0.3	1418.36	1419.54	1418.67	1419.55	0.000102	0.48	0.63	0.52	0.14
125	Max flow	0.3	1418.23	1419.51	1418.54	1419.52	0.000082	0.43	0.7	0.9	0.12
124	Max flow	0.3	1418.07	1419.5	1418.38	1419.51	0.000031	0.34	0.88	1.2	0.09
123	Max flow	0.3	1417.92	1419.5	1418.22	1419.5	0.000026	0.29	1.05	1.2	0.07
122	Max flow	0.3	1417.76	1419.49	1418.07	1419.49	0.000058	0.24	1.23	1.2	0.06

River Station	Profile	Q Total	Min Ch El	W.S. Elev	Crit W.S.	E.G. Elev	E.G. Slope	Vel Chnl	Flow Area	Top Width	Froude # Canal
121	Max flow	0.3	1417.61	1419.46	1417.92	1419.47	0.000103	0.22	1.38	1.2	0.05
120	Max flow	0.3	1417.45	1419.42	1417.76	1419.42	0.000242	0.2	1.52	1.2	0.04
119	Max flow	0.3	1417.3	1419.33	1417.6	1419.33	0.00037	0.19	1.6	1.2	0.04
118	Max flow	0.3	1417.14	1419.26	1417.45	1419.26	0.000167	0.18	1.7	1.2	0.04
117	Max flow	0.3	1416.99	1419.17	1417.29	1419.17	0.000726	0.17	1.77	1.2	0.04
116	Max flow	0.3	1416.83	1419.01	1417.14	1419.02	0.00038	0.17	1.78	1.2	0.04
115	Max flow	0.3	1416.68	1418.86	1416.99	1418.86	0.000721	0.17	1.78	1.2	0.04
114	Max flow	0.3	1416.52	1418.71	1416.83	1418.71	0.000376	0.17	1.78	1.2	0.04
113	Max flow	0.3	1416.37	1418.56	1416.67	1418.56	0.000712	0.17	1.78	1.2	0.04
112	Max flow	0.3	1416.21	1418.4	1416.52	1418.4	0.000419	0.17	1.78	1.2	0.04
111	Max flow	0.3	1416.06	1418.23	1416.37	1418.24	0.000731	0.17	1.77	1.2	0.04
110	Max flow	0.3	1415.9	1418.08	1416.21	1418.08	0.000385	0.17	1.77	1.2	0.04
109	Max flow	0.3	1415.75	1417.92	1416.05	1417.93	0.000732	0.17	1.77	1.2	0.04
108	Max flow	0.3	1415.59	1417.77	1415.9	1417.77	0.000385	0.17	1.77	1.2	0.04
107	Max flow	0.3	1415.44	1417.61	1415.75	1417.62	0.000732	0.17	1.77	1.2	0.04
106	Max flow	0.3	1415.28	1417.46	1415.59	1417.46	0.000386	0.17	1.77	1.2	0.04
105	Max flow	0.3	1415.13	1417.3	1415.44	1417.31	0.000733	0.17	1.77	1.2	0.04
104	Max flow	0.3	1414.97	1417.15	1415.28	1417.15	0.000386	0.17	1.77	1.2	0.04
103	Max flow	0.3	1414.82	1416.99	1415.12	1416.99	0.000734	0.17	1.76	1.2	0.04
102	Max flow	0.3	1414.66	1416.84	1414.97	1416.84	0.000387	0.17	1.77	1.2	0.04
101	Max flow	0.3	1414.51	1416.68	1414.81	1416.68	0.000736	0.17	1.76	1.2	0.04
100	Max flow	0.3	1414.35	1416.52	1414.66	1416.53	0.000389	0.17	1.76	1.2	0.04
99	Max flow	0.3	1414.2	1416.37	1414.5	1416.37	0.000742	0.17	1.76	1.2	0.04
98	Max flow	0.3	1414.04	1416.21	1414.35	1416.21	0.000393	0.17	1.76	1.2	0.04
97	Max flow	0.3	1413.89	1416.05	1414.2	1416.05	0.00075	0.17	1.75	1.2	0.04
96	Max flow	0.3	1413.73	1415.89	1414.04	1415.89	0.000401	0.17	1.75	1.2	0.04
95	Max flow	0.3	1413.58	1415.73	1413.89	1415.73	0.00077	0.17	1.74	1.2	0.04
94	Max flow	0.3	1413.42	1415.57	1413.73	1415.57	0.000383	0.17	1.74	1.2	0.04
93	Max flow	0.3	1413.27	1415.42	1413.58	1415.42	0.000718	0.17	1.73	1.2	0.04

River Station	Profile	Q Total	Min Ch El	W.S. Elev	Crit W.S.	E.G. Elev	E.G. Slope	Vel Chnl	Flow Area	Top Width	Froude # Canal
92	Max flow	0.3	1413.11	1415.28	1413.42	1415.29	0.000299	0.17	1.76	1.2	0.04
91	Max flow	0.3	1412.97	1415.14	1413.27	1415.14	0.000853	0.17	1.77	1.2	0.04
90	Max flow	0.3	1412.95	1414.21	1413.26	1414.22	0.31069	0.44	0.68	0.75	0.13
89	Max flow	0.3	1412.93	1414.22		1414.22	0	0.13	2.35	2.76	0.04
88	Max flow	0.3	1412.87	1414.22		1414.22	0.000002	0.12	2.52	2.82	0.04
87	Max flow	0.3	1412.81	1414.22		1414.22	0	0.11	2.69	2.88	0.04
86	Max flow	0.3	1412.75	1414.22		1414.22	0.000004	0.1	2.87	2.95	0.03
85	Max flow	0.3	1412.69	1414.22		1414.22	0.000367	0.1	3.04	3.03	0.03
84	Max flow	0.3	1412.63	1414.15		1414.15	0.000538	0.1	3.02	3.02	0.03
83	Max flow	0.3	1412.57	1414.07		1414.07	0.000572	0.1	2.95	2.99	0.03
82	Max flow	0.3	1412.51	1414		1414	0.000411	0.1	2.91	2.97	0.03
81	Max flow	0.3	1412.45	1413.93		1413.93	0.000413	0.1	2.91	2.97	0.03
80	Max flow	0.3	1412.39	1413.86		1413.86	0.000619	0.1	2.86	2.95	0.03
79	Max flow	0.3	1412.33	1413.76		1413.76	0.000687	0.11	2.75	2.91	0.04
78	Max flow	0.3	1412.27	1413.65		1413.65	0.000795	0.12	2.61	2.86	0.04
77	Max flow	0.3	1412.21	1413.54		1413.54	0.000634	0.12	2.48	2.81	0.04
76	Max flow	0.3	1412.15	1413.44		1413.44	0.000719	0.13	2.36	2.76	0.04
75	Max flow	0.3	1412.09	1413.32		1413.33	0.000864	0.14	2.2	2.68	0.05
74.5	Max flow	0.3	1412.06	1413.27	1412.16	1413.27	0.000191	0.07	4.08	3.45	0.02
74.4		Inl Struct									
74	Max flow	0.3	1412.03	1413.27		1413.27	0	0.14	2.22	2.69	0.05
73	Max flow	0.3	1411.97	1413.27		1413.27	0	0.13	2.38	2.77	0.04
72	Max flow	0.3	1411.91	1413.27		1413.27	0	0.12	2.55	2.83	0.04
71	Max flow	0.3	1411.85	1413.27		1413.27	0	0.11	2.72	2.89	0.04
70	Max flow	0.3	1411.79	1413.27		1413.27	0.000417	0.1	2.9	2.96	0.03
69	Max flow	0.3	1411.73	1413.21		1413.21	0.000421	0.1	2.89	2.96	0.03
68	Max flow	0.3	1411.67	1413.14		1413.14	0.000425	0.1	2.88	2.95	0.03
67	Max flow	0.3	1411.61	1413.08		1413.08	0.000429	0.1	2.87	2.95	0.03
66	Max flow	0.3	1411.55	1413		1413	0.00065	0.11	2.81	2.93	0.03

River Station	Profile	Q Total	Min Ch El	W.S. Elev	Crit W.S.	E.G. Elev	E.G. Slope	Vel Chnl	Flow Area	Top Width	Froude # Canal
65	Max flow	0.3	1411.49	1412.86		1412.86	0.001601	0.12	2.57	2.84	0.04
64	Max flow	0.3	1411.43	1412.69		1412.69	0.000793	0.13	2.28	2.72	0.05
63	Max flow	0.3	1411.37	1412.56		1412.56	0.001013	0.14	2.08	2.63	0.05
62	Max flow	0.3	1411.31	1412.22		1412.22	0.008329	0.22	1.39	2.32	0.09
61.5	Max flow	0.3	1411.28	1412.18	1411.38	1412.18	0.000449	0.1	3.01	3.41	0.03
61.4		Inl Struct									
61	Max flow	0.3	1411.25	1412.16	1411.55	1412.18	0.000112	0.54	0.56	0.12	0.18
60	Max flow	0.3	1411.04	1412.12	1411.35	1412.13	0.000144	0.51	0.59	0.3	0.16
59	Max flow	0.3	1410.84	1412.1	1411.15	1412.11	0.000043	0.44	0.68	0.75	0.13
58	Max flow	0.3	1410.73	1412.09	1411.04	1412.1	0.000015	0.38	0.79	1.2	0.1
57	Max flow	0.3	1410.64	1412.09	1410.94	1412.1	0.00002	0.33	0.9	1.2	0.09
56	Max flow	0.3	1410.43	1412.08	1410.74	1412.09	0.000025	0.26	1.14	1.2	0.07
55	Max flow	0.3	1410.23	1412.08	1410.54	1412.08	0.000013	0.22	1.37	1.2	0.05
54	Max flow	0.3	1410.03	1412.07	1410.34	1412.08	0.000016	0.19	1.61	1.2	0.04
53	Max flow	0.3	1409.82	1412.06	1410.13	1412.06	0.000442	0.16	1.84	1.2	0.03
52	Max flow	0.3	1409.62	1411.89	1409.93	1411.89	0.000583	0.16	1.87	1.2	0.03
51	Max flow	0.3	1409.42	1411.68	1409.73	1411.69	0.000576	0.16	1.88	1.2	0.03
50	Max flow	0.3	1409.27	1411.57	1409.58	1411.57	0.000219	0.16	1.92	1.2	0.03
49	Max flow	0.3	1409.07	1411.42	1409.37	1411.42	0.001178	0.15	1.98	1.2	0.03
48	Max flow	0.3	1408.86	1410.01	1409.17	1410.02	0.197003	0.49	0.62	0.45	0.15
47	Max flow	0.3	1408.76	1409.92		1409.92	0.000362	0.15	2	2.61	0.05
46	Max flow	0.3	1408.68	1409.87		1409.87	0.000322	0.14	2.08	2.64	0.05
45	Max flow	0.3	1408.59	1409.87		1409.87	0	0.13	2.31	2.74	0.05
44	Max flow	0.3	1408.51	1409.87		1409.87	0.000585	0.12	2.55	2.84	0.04
43	Max flow	0.3	1408.42	1409.78		1409.79	0.000591	0.12	2.54	2.83	0.04
42	Max flow	0.3	1408.34	1409.74		1409.74	0.000168	0.11	2.66	2.88	0.04
41	Max flow	0.3	1408.25	1409.74		1409.74	0.000001	0.1	2.91	2.98	0.03
40.5	Max flow	0.3	1408.23	1409.74	1408.33	1409.74	0.000015	0.06	5.13	3.49	0.02

River Station	Profile	Q Total	Min Ch El	W.S. Elev	Crit W.S.	E.G. Elev	E.G. Slope	Vel Chnl	Flow Area	Top Width	Froude # Canal
40.4		Inl Struct									
40	Max flow	0.3	1408.17	1409.74		1409.74	0	0.09	3.16	3.1	0.03
39	Max flow	0.3	1408.08	1409.74		1409.74	0.000386	0.09	3.42	3.1	0.03
38	Max flow	0.3	1408	1409.69		1409.69	0.000244	0.08	3.54	3.1	0.03
37	Max flow	0.3	1407.91	1409.67		1409.67	0.000094	0.08	3.74	3.1	0.02
36	Max flow	0.3	1407.83	1409.64		1409.64	0.001025	0.08	3.9	3.1	0.02
35	Max flow	0.3	1407.74	1409.47		1409.47	0.001232	0.08	3.64	3.1	0.02
34	Max flow	0.3	1407.66	1409.26		1409.26	0.001697	0.09	3.24	3.1	0.03
33	Max flow	0.3	1407.57	1408.9		1408.9	0.003623	0.12	2.43	2.79	0.04
32	Max flow	0.3	1407.49	1408.51		1408.51	0.001901	0.18	1.65	2.46	0.07
31	Max flow	0.3	1407.4	1408.4		1408.4	0.0004	0.19	1.58	2.43	0.08
30	Max flow	0.3	1407.32	1408.34		1408.34	0.000356	0.18	1.65	2.46	0.07
29	Max flow	0.3	1407.23	1408.29		1408.29	0.00031	0.17	1.74	2.51	0.07
28	Max flow	0.3	1407.15	1408.29		1408.29	0.000001	0.15	1.95	2.59	0.06
27	Max flow	0.3	1407.06	1408.29		1408.29	0.000288	0.14	2.17	2.67	0.05
26	Max flow	0.3	1406.98	1408.25		1408.25	0.000249	0.13	2.29	2.73	0.05
25	Max flow	0.3	1406.89	1408.2		1408.2	0.000444	0.13	2.39	2.78	0.04
24	Max flow	0.3	1406.81	1408.12		1408.12	0.000686	0.12	2.4	2.78	0.04
23	Max flow	0.3	1406.72	1408.01		1408.02	0.000733	0.13	2.34	2.75	0.04
22	Max flow	0.3	1406.64	1407.9		1407.9	0.000807	0.13	2.26	2.71	0.05
21	Max flow	0.3	1406.55	1407.77		1407.77	0.000934	0.14	2.14	2.66	0.05
20	Max flow	0.3	1406.47	1407.49		1407.49	0.0053	0.18	1.64	2.46	0.07
19	Max flow	0.3	1406.38	1407		1407	0.0022	0.4	0.75	1.89	0.2
18.5	Max flow	0.3	1406.37	1407	1406.46	1407	0	0.14	2.12	3.38	0.06
18.4		Inl Struct									
18	Max flow	0.3	1406.3	1406.74		1406.77	0.000119	0.66	0.46	1.59	0.39
17	Max flow	0.3	1406.21	1406.74		1406.75	0.000058	0.51	0.59	1.74	0.28
16	Max flow	0.3	1406.13	1406.74		1406.75	0.000022	0.4	0.75	1.89	0.2

River Station	Profile	Q Total	Min Ch El	W.S. Elev	Crit W.S.	E.G. Elev	E.G. Slope	Vel Chnl	Flow Area	Top Width	Froude # Canal
15	Max flow	0.3	1406.04	1406.73		1406.74	0.001327	0.33	0.9	2.01	0.16
14	Max flow	0.3	1405.96	1406.57		1406.58	0.000913	0.41	0.74	1.88	0.21
13	Max flow	0.3	1405.87	1406.48		1406.49	0.000403	0.41	0.73	1.87	0.21
12	Max flow	0.3	1405.79	1406.47		1406.47	0.000043	0.34	0.88	1.99	0.17
11	Max flow	0.3	1405.79	1406.46		1406.47	0.000044	0.35	0.86	1.98	0.17
10	Max flow	0.3	1405.7	1406.46		1406.47	0	0.29	1.04	2.11	0.13
9	Max flow	0.3	1405.62	1406.46		1406.47	0.000117	0.24	1.23	2.23	0.11
8	Max flow	0.3	1405.45	1406.43		1406.44	0.000416	0.19	1.56	2.41	0.08
7	Max flow	0.3	1405.36	1406.43		1406.43	0.000016	0.17	1.75	2.51	0.07
6	Max flow	0.3	1405.28	1406.43		1406.43	0	0.15	1.97	2.6	0.06
5	Max flow	0.3	1405.19	1406.43		1406.43	0.000875	0.14	2.19	2.68	0.05
4	Max flow	0.3	1405.09	1406.29		1406.29	0.001002	0.14	2.08	2.64	0.05
3	Max flow	0.3	1405	1406.23		1406.23	0.000224	0.14	2.17	2.67	0.05
2	Max flow	0.3	1404.98	1406.19		1406.19	0.000236	0.14	2.13	2.65	0.05
1.5	Max flow	0.3	1404.89	1406.19	1404.99	1406.19	0.000039	0.07	4.39	3.47	0.02
1.4		Inl Struct									
1	Max flow	0.3	1404.85	1406.19		1406.19	0.000228	0.12	2.48	2.81	0.04
0	Max flow	0.3	1404.77	1406.14	1405.05	1406.14	0.000581	0.12	2.56	2.84	0.04